

## Article

# Hybrid Materials Based on Imidazo[4,5-*b*]porphyrins for Catalytic Oxidation of Sulfides

Inna A. Abdulaeva <sup>1,2</sup>, Kirill P. Birin <sup>2,\*</sup> , Remi Chassagnon <sup>3</sup>  and Alla Bessmertnykh-Lemeune <sup>1,4,\*</sup> 

<sup>1</sup> Institut de Chimie Moléculaire de l'Université de Bourgogne, UMR CNRS 6302, Université Bourgogne Franche-Comté, 9 Avenue Alain Savary, 21078 Dijon, France

<sup>2</sup> Frumkin Institute of Physical Chemistry and Electrochemistry, Russian Academy of Sciences, Leninsky Pr. 31-4, 119071 Moscow, Russia

<sup>3</sup> Laboratoire Interdisciplinaire Carnot de Bourgogne, UMR CNRS 6303, Université Bourgogne Franche-Comté, 9 Avenue Alain Savary, 21078 Dijon, France

<sup>4</sup> ENS de Lyon, UMR 5182, CNRS, Laboratoire de Chimie, 69342 Lyon, France

\* Correspondence: kirill.birin@gmail.com (K.P.B.); alla.lemeune@ens-lyon.fr (A.B.-L.)

**Abstract:** Heterogenized metalloporphyrin catalysts for oxidation reactions are extensively explored to improve chemical production. In this work, manganese *meso*-tetraarylporphyrins were immobilized on hydrated mesoporous titanium dioxide ( $S_{\text{BET}} = 705 \text{ m}^2 \text{ g}^{-1}$ ) through carboxylate or phosphonate anchoring groups separated from the macrocycle by the 2-arylimidazole linker fused across one of the pyrrolic rings of the macrocycle. The element composition of two mesoporous hybrid materials thus obtained were investigated and the integrity of the immobilized complexes was shown by different physicochemical methods. Finally, the catalytic efficiency of the more stable material **Mn(TMPIP)/TiO<sub>2</sub>** with the phosphonate anchor was evaluated in the selective oxidation of sulfides to sulfoxides by molecular oxygen in the presence of isobutyraldehyde (IBA). The heterogenized complex has shown excellent catalytic activity exhibiting a turnover (TON) of ~1100 in a single catalytic run of the sulfoxidation of thioanisole. The catalyst was successfully reused in seven consecutive catalytic cycles.

**Keywords:** metalloporphyrin; titania; heterogenized catalyst; oxidation



**Citation:** Abdulaeva, I.A.; Birin, K.P.;

Chassagnon, R.; Bessmertnykh-

Lemeune, A. Hybrid Materials Based

on Imidazo[4,5-*b*]porphyrins for

Catalytic Oxidation of Sulfides.

*Catalysts* **2023**, *13*, 402. [https://](https://doi.org/10.3390/catal13020402)

[doi.org/10.3390/catal13020402](https://doi.org/10.3390/catal13020402)

Academic Editor: Roman Bulánek

Received: 31 December 2022

Revised: 3 February 2023

Accepted: 9 February 2023

Published: 13 February 2023



**Copyright:** © 2023 by the authors.

Licensee MDPI, Basel, Switzerland.

This article is an open access article

distributed under the terms and

conditions of the Creative Commons

Attribution (CC BY) license ([https://](https://creativecommons.org/licenses/by/4.0/)

[creativecommons.org/licenses/by/](https://creativecommons.org/licenses/by/4.0/)

[4.0/](https://creativecommons.org/licenses/by/4.0/)).

## 1. Introduction

Oxidation reactions are key technological processes for converting petroleum into pharmaceuticals, agrochemicals, and fine chemicals [1,2]. Among all transformations of organic compounds, oxidation reactions are especially challenging because they often have low selectivity and require stoichiometric amounts of toxic and hazardous oxidizing reagents such as oxometal oxidants or peracids [3]. Thus, these processes are among the most dangerous and pollutant transformations in chemical production. The development of reactions in which molecular oxygen is used as a terminal oxidant, together with a reusable catalyst and a nontoxic solvent, is extremely important for both economic and environmental reasons [4]. It is not surprising that catalytic aerobic oxidation reactions performed with both non-metal and metal catalysts have received great attention [5,6].

In nature, such processes are carried out in a highly selective manner by mono- and dioxygenases under mild conditions [7,8]. This stimulated investigations of biomimetic porphyrin catalysts pioneered by Groves and co-workers, who studied the oxidation of organic compounds by strong oxidants in the presence of iron(III) porphyrinates in the late seventies of the last century [9–11]. Later extensive studies on the metalloporphyrin-catalyzed oxidation have demonstrated that the catalytic efficiency of manganese(III), ruthenium(III) and cobalt(III) porphyrins can even exceed that of iron(III) complexes in part due to the high stability of these complexes [12–16]. Another remarkable feature of metalloporphyrins is that these catalysts are efficient in different types of oxidation

processes, such as the epoxidation and hydration of alkenes, the hydroxylation of alkanes, the dehydrogenation of amines, and the oxidation of arenes, amines, sulfides, alcohols, and aldehydes and so forth [8,17]. The reaction rate and selectivity can be controlled by varying the nature of the central metal ion and substituents at the periphery of the porphyrin macrocycle. The peripheral substituents also influence the catalyst stability, and *meso*-tetraarylporphyrins bearing *ortho*-disubstituted aryl residues and electron-deficient aryl groups exhibit high efficiency in part due to their increased chemical stability [18,19]. Lately, major interest in these reactions appeared when it was shown that metalloporphyrins could catalyze reactions with environment-friendly oxidants such as hydrogen peroxide or molecular oxygen which can be used in the presence of isobutyraldehyde (IBA) as a sacrificial reagent or in photooxidation processes [8].

Unfortunately, the use of metalloporphyrins in practical organic synthesis is still limited because these catalysts are expensive and often have a disappointingly low TON and TOF. It was recognized that the heterogenization of homogeneous catalysts significantly increased their efficiency. In fact, solid catalysts based on metalloporphyrins commonly display higher stability than their homogeneous counterparts because the deactivation of metalloporphyrin catalysts mainly proceeds through the formation of catalytically inactive dimeric complexes. The catalyst dimerization can be decreased when porphyrin molecules are attached to a solid support, in particular through covalent bonding [20]. Being heterogenized, the expensive metalloporphyrins can be recovered after the reaction completion and reused in the next catalytic cycle. This simplifies product isolation and could decrease the cost of industrial production. Thus, recent research was mainly focused on preparing efficient heterogenized porphyrin catalysts [21].

Several different strategies were investigated for the immobilization of porphyrin complexes onto inorganic and organic supports [22–29], such as zeolites [30,31], clays [32–35], silicas [36–39], polymers [20,40], metal-organic frameworks (MOF) [21,41–44] and covalent organic frameworks (COF) [45]. Metalloporphyrin catalysts were also grafted onto photoactive anatase and a nanocrystalline anatase/hydrozincite composite material using triethoxysilane anchoring group [46] or electrostatic interactions [47], respectively. Surprisingly, the photocatalytic decomposition of porphyrins immobilized on these photoactive supports was slow, and the materials thus obtained were stable enough to be used as reusable catalysts. Recently, the method for the preparation of hybrid materials bearing two porphyrin complexes incorporated into charged layer supports was developed [47,48]. Most of the previously reported heterogenized complexes were efficient as catalysts, and a synergistic action of support and transition metal catalysts was observed in some cases [43,44,48]. It was also shown that the immobilization of metalloporphyrin catalysts could switch the chemoselectivity of oxidation reactions [47,49].

Porous materials with high surface areas are widely explored in catalysis because they allow us to increase catalyst loading and diminish the influence of the physical phenomenon of mass transfer on reaction rates [50,51]. Different types of porous materials were investigated, but all of them have serious drawbacks. Mesoporous silicas commonly display low chemical stability [52,53]. MOF- and COF-bearing catalytic centers in porphyrinic linkers are expensive because a high amount of metalloporphyrins is required for their preparation, and drying procedures leading to porous crystalline networks are very troublesome and time-consuming [54]. Microporous zeolites are also inconvenient as solid supports for porphyrins because the size of porphyrin molecules is close to that of most available zeolite Y supercages (~1.3 nm in diameter) and the diffusion of organic compounds through zeolite lattice apertures is sterically hindered in these hybrid materials [55]. There is, thus, a need for more efficient immobilization strategies for preparing porous catalysts based on metalloporphyrins.

In this work, we report grafting porphyrin complexes on the surface of hydrated mesoporous titanium(IV) oxide (TiO<sub>2</sub>,  $S_{\text{BET}} = 650\text{--}705 \text{ m}^2 \text{ g}^{-1}$ ). This cheap and photocatalytically inactive support was recently prepared by us using a non-templating sol-gel

process. Our grafting methodology is based on the use of imidazo[4,5-*b*]porphyrins as molecular precursors (Figure 1). These fused porphyrin-heterocycle compounds, which were pioneered by Crossley et al. [56], were widely studied but were not used for the preparation of heterogenized catalysts [57]. The 2-aryl-imidazole residue is of interest as a linker in the synthesis of functional materials because the introduction of different substituents in the aryl residue of this linker is straightforward [56,58]. This long and rigid spacer provides a perpendicular orientation of the porphyrin ring with respect to the solid surface. The synthetic strategy based on the introduction of the 2-arylimidazole residue fused across one pyrrolic ring of the macrocycle opens a way for covalent grafting *meso*-tetraarylporphyrins, in particular their derivatives with sterically hindered *o*-disubstituted aryl groups which are known to be most efficient catalysts for the oxidation reactions [59]. In this work, this strategy was used for grafting porphyrin catalysts onto titanium dioxide through a carboxylate or phosphonate anchoring group, as shown in Figure 1. The element composition of two mesoporous hybrid materials thus obtained were investigated, and the integrity of the immobilized molecules was shown using different physicochemical techniques. Finally, the catalytic efficiency of the more stable material **Mn(TMPIP)/TiO<sub>2</sub>** was evaluated in the selective oxidation of sulfides to sulfoxides by molecular oxygen in the presence of IBA. The **Mn(TMPIP)/TiO<sub>2</sub>** material has shown excellent catalytic activity and was successfully reused in seven catalytic cycles.

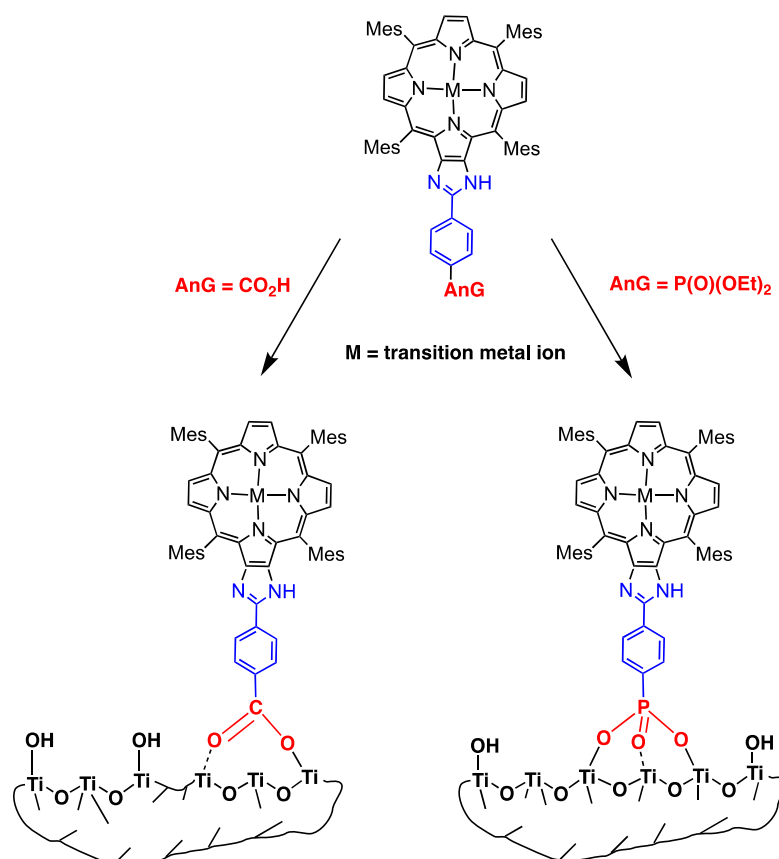


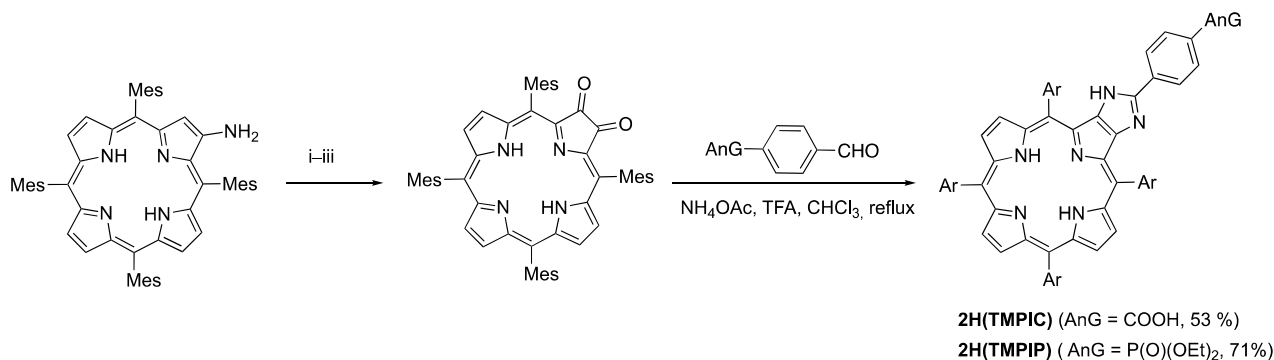
**Figure 1.** Strategies for the immobilization of porphyrin catalysts on hydrated titania supports, which were investigated in this work.

## 2. Results and Discussion

### 2.1. Synthesis of (2-arylimidazo[4,5-*b*]porphyrinato)manganese(III) Chlorides and Their Characterization

*meso*-Tetramesityl-substituted imidazo[4,5-*b*]porphyrins were chosen for investigation in this work as their synthesis is reproducible, and they can be obtained in a 100 milligram scale using available laboratory equipment. The free base 2-arylimidazo[4,5-*b*]porphyrins

**2H(TMPIC)** and **2H(TMPIP)** bearing carboxylate and phosphonate anchoring groups on the aryl substituent of imidazole were prepared through the oxidation of corresponding  $\beta$ -aminoporphyrin to 2,3-dioxochlorin followed by the Debus–Radziszewski condensation of this dione with aromatic aldehydes (Scheme 1) [58].



**Scheme 1.** Synthesis of **2H(TMPIC)** and **2H(TMPIP)**. General conditions and reagents: (i)  $\text{Cu}(\text{NO}_3)_2$ , acetic anhydride, 40 °C, 30 min; (ii)  $\text{H}_2\text{SO}_4$  + TFA,  $\text{CH}_2\text{Cl}_2$ , r.t., 2.5 h; (iii)  $\text{SnCl}_2 \cdot 2\text{H}_2\text{O}$ , HCl,  $\text{CH}_2\text{Cl}_2$ , r.t., 2.5 h.

Insertion of manganese ions was carried out using synthetic procedures developed for 5,10,15,20-tetraphenylporphyrin [60]. Free base porphyrins **2H(TMPIC)** and **2H(TMPIP)** were heated with an excess of manganese(II) chloride (five equiv equivalents) in DMF under air until the complete consumption of the starting compound. Complexes **Mn(TMPIC)** and **Mn(TMPIP)** were isolated by column chromatography on silica gel and characterized by HRMS-ESI spectrometry, FTIR and UV-vis spectroscopies, with the last one being the most useful spectroscopic technique. The complexes display UV-vis spectra characteristic of manganese(III) porphyrins showing specific shapes compared to other porphyrin complexes due to strong metal-porphyrin  $\pi$  interactions [61,62]. The mixing of metal and porphyrin orbitals leads to the appearance of a number of charge-transfer bands which alter classical electron absorption spectra of the porphyrin complexes in which only  $\pi$ - $\pi^*$  transitions of the macrocycle are observed. For example, in the spectrum of **Mn(TMPIP)** in  $\text{CHCl}_3$ , several bands appear in the region of 300–450 nm with the maxima at 312, 382, and 402 nm (the region of VI and V bands) and a sharp charge-transfer band is observed at 484 nm ( $\log \epsilon = 4.92$ , V band; see Supporting Information (SI), Figure S1). Moreover, less intensive bands appear at 576 nm (IV band) and 622 (III band) and 749 (II band). The successful insertion of manganese ion was also confirmed by observation of  $[\text{M}+\text{H}]^+$ ,  $[\text{M}-\text{Cl}]^+$  and  $[\text{M}-\text{Cl}+\text{H}]^{2+}$  ion peaks with matching isotopic patterns as the most prominent peaks in the high-resolution mass spectra of complexes **Mn(TMPIP)** and **Mn(TMPIC)** (see Supplementary Materials, Figures S2 and S3).

DFT calculations were employed to gain insight into electronic structures for the frontier orbitals of complexes **Mn(TMPIC)** and **Mn(TMPIP)** and (5,10,15,20-tetraphenylporphyrinato)manganese(III) chloride (**Mn(TPP)**). The computations were performed using B3LYP functional using 6-31G\* basis set for all atoms, including all-electron set for Mn. As shown in Figure 2, efficient mixing of metal and porphyrin orbitals is observed in HOMO and LUMO orbitals. In complexes **Mn(TMPIC)** and **Mn(TMPIP)**, the electronic density of HOMO is also located on the fused imidazole fragment. In contrast, the 2-aryl residue is not involved in the HOMO and LUMO electronic states of both imidazoporphyrins. Thus, the introduction of any anchoring group does not significantly change the electronic structure of 2-arylimidazo[4,5-*b*]porphyrins and energies of frontier molecular orbitals. This appears to indicate that electronic communication between the catalytic site and any solid support may be weak when a 2-arylimidazole linker is used for preparing heterogenized catalysts.

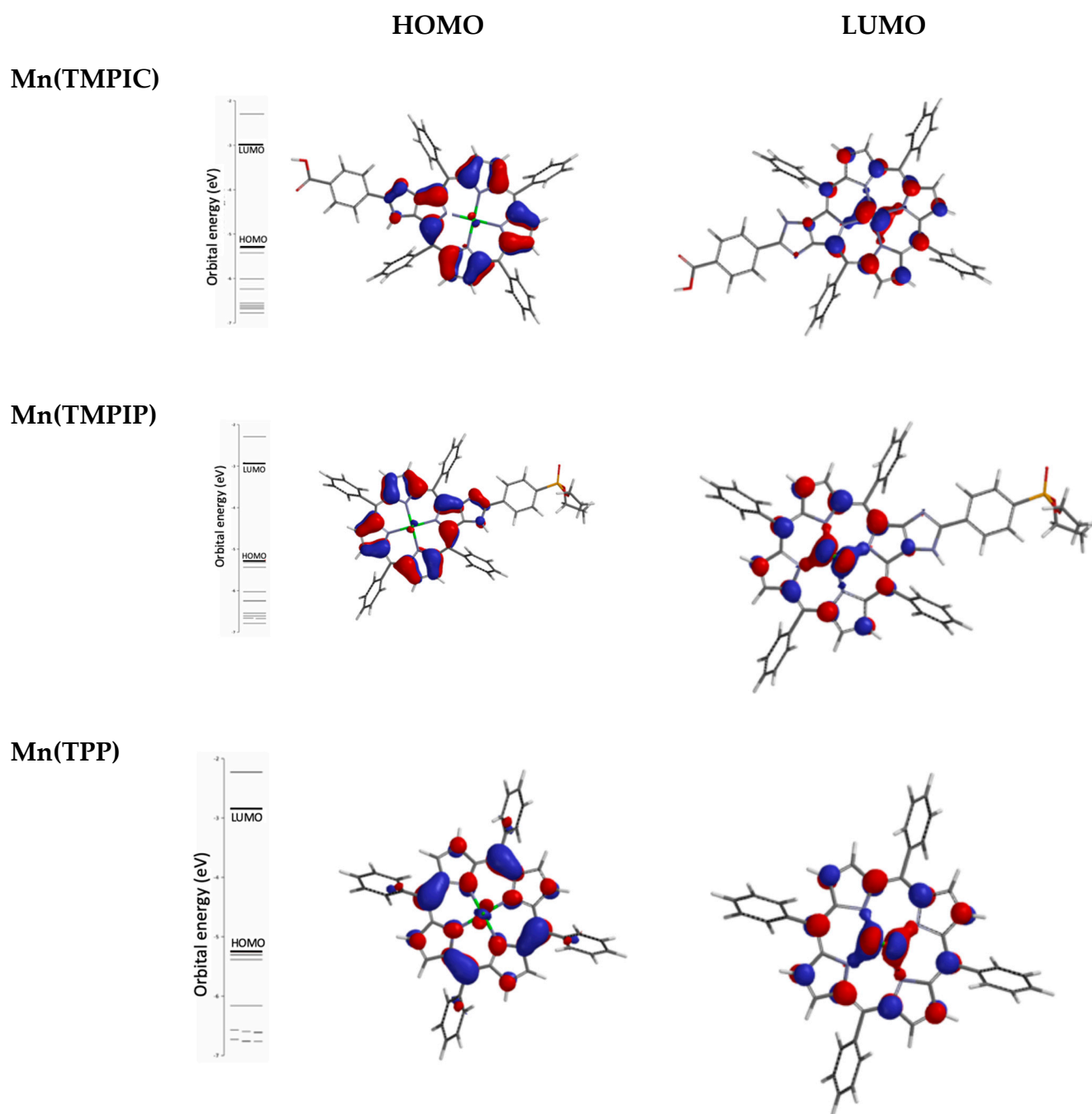


**Figure 2.** The isodensity plot of HOMO and LUMO orbitals for porphyrins **Mn(TPP)**, **Mn(TMPIC)** and **Mn(TMPIP)** obtained from DFT calculations.

Complexes **Mn(TMPIC)** and **Mn(TMPIP)** were found to be soluble in methanol and chlorinated solvents such as chloroform and dichloromethane, which is important for their use in material chemistry.

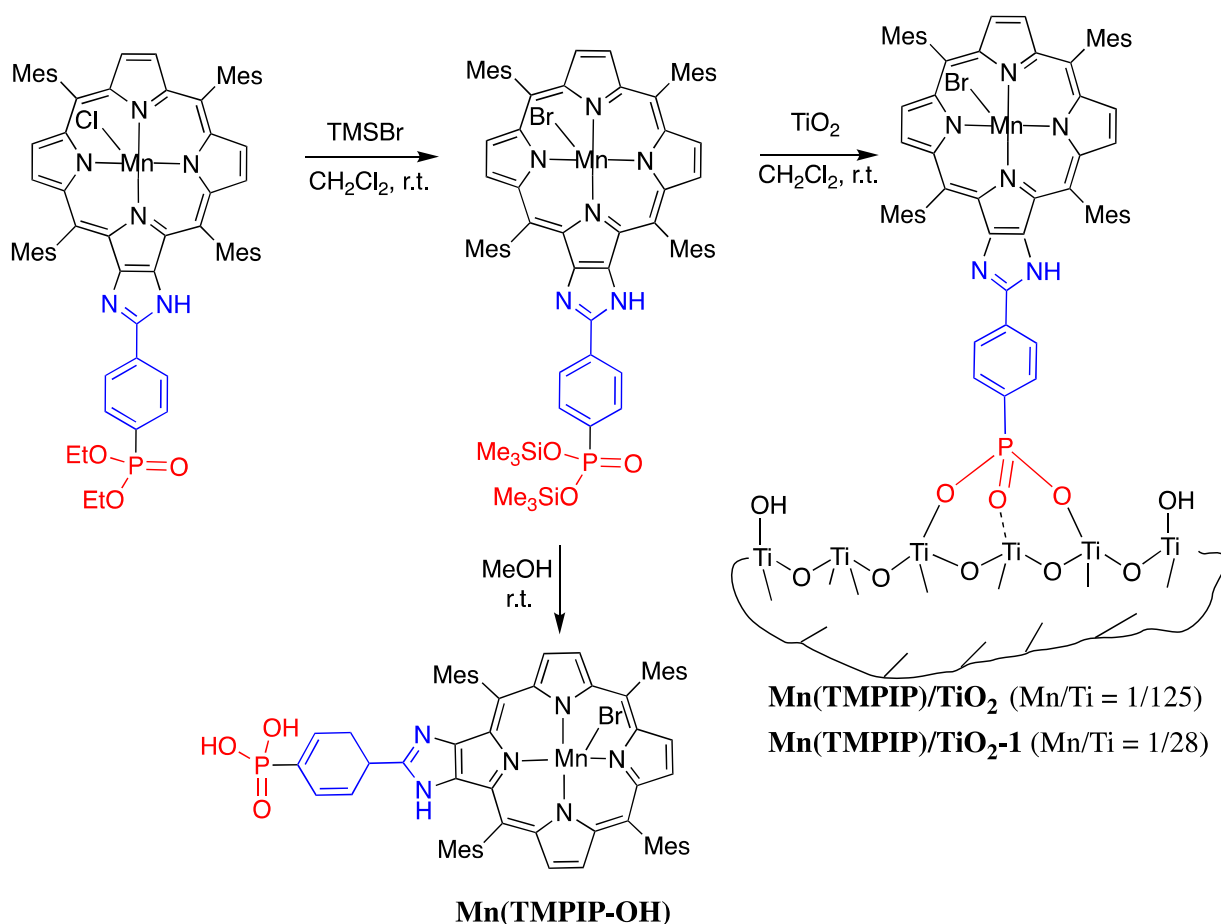
## 2.2. Immobilization of Manganese(III) Complexes *Mn(TMPIC)* and *Mn(TMPIP)* on $\text{TiO}_2$

Recent studies of hybrid organic-inorganic materials based on organophosphonates have revealed the great potential of metal oxide and phosphonate networks for preparing functional materials, in particular, due to their thermal and chemical stability [63–66]. Nevertheless, studies on  $\text{TiO}_2$ -supported transition metal catalysts are limited [67–74], probably because the synthesis of porous  $\text{TiO}_2$  is challenging and time-consuming. On the

other hand, the immobilization of organic chromophores onto porous titania films was widely explored in view of the production of clean energy from the sun in dye-sensitized solar cells [75]. Among different anchors, the carboxylate group was most commonly used and sometimes gave better results as compared to the phosphonate anchoring group. In this work, we compared the efficiency of the carboxylate and phosphonate anchors for the fabrication of heterogenized catalysts.

**Mn(TMPIC)** and **Mn(TMPIP)** were grafted onto the surface of hydrated amorphous titanium dioxide, which does not exhibit any photocatalytic activity on its own. Such cost-effective mesoporous  $\text{TiO}_2$  ( $S_{\text{BET}} = 650\text{--}705 \text{ m}^2 \text{ g}^{-1}$ ) is readily available by a template-free sol-gel method developed by us recently [76].

To prepare target materials from phosphonate-substituted complex **Mn(TMPIP)**, we employed a sol-gel process in organic solvents [77,78] since the immobilization of phosphonic acids in aqueous media probably occurs through monodentate P–O–Ti interactions and yields less-stable materials [71]. Dialkyl phosphoester **Mn(TMPIP)** was first transformed into more reactive bis(trimethylsilyl)phosphonate by reacting the complex with a large excess (30 equivalents; a large excess was used to accelerate the reaction performed in a diluted solution) of bromotrimethylsilane (TMSBr) in  $\text{CH}_2\text{Cl}_2$  for 2 d at room temperature (Scheme 2). The evaporation of the reaction mixture to dryness gave the target compound in a quantitative yield.



**Scheme 2.** Preparation of materials Mn(TMPIP)/TiO<sub>2</sub> and Mn(TMPIP)/TiO<sub>2</sub>-1.

Then this moisture-sensitive complex was engaged in the next step, dissolving the solid in dry  $\text{CH}_2\text{Cl}_2$  and adding this solution to a suspension of mesoporous titania in the same solvent at room temperature under Ar. The material was isolated by centrifugation after stirring for 2 d, thoroughly washed with THF, water, MeOH, and ether and dried under reduced pressure. In these experiments, the Mn/Ti molar ratio was varied

between 1:100 and 1:15 to prepare a solid with spatially separated catalytic sites (1:100,  $\text{Mn}(\text{TMPIP})/\text{TiO}_2$ ) and to get insight into maximal loading of catalytic sites on this support (1:15,  $\text{Mn}(\text{TMPIP})/\text{TiO}_2\text{-1}$ ).

The studies on the element composition of hybrid materials thus obtained were started by EDX chemical analysis in STEM mode of solid  $\text{Mn}(\text{TMPIP})/\text{TiO}_2$  because this technique is well suited for the determination of the axial ligand in the heterogenized  $\text{Mn}(\text{TMPIP})$ . It was previously demonstrated that the treatment of porphyrinatogallium(III) chlorides with TMSBr in toluene led to the exchange of axial chloride ligands by bromide ions [79]. We hypothesized that this exchange reaction could also be observed under our experimental conditions. The EDX spectrum confirmed successful grafting of the Mn complex and the presence of all expected elements, with the only exception being chlorine (Figures 3 and S5 (see Supplementary Materials)). We also observed an EDX peak corresponding to bromine. This indicated that the ligand exchange reaction was observed during the activation of the diethoxyphosphoryl group by TMSBr. The elemental mapping images shown in Figure 3 revealed the homogeneous distribution of all elements in the studied samples.

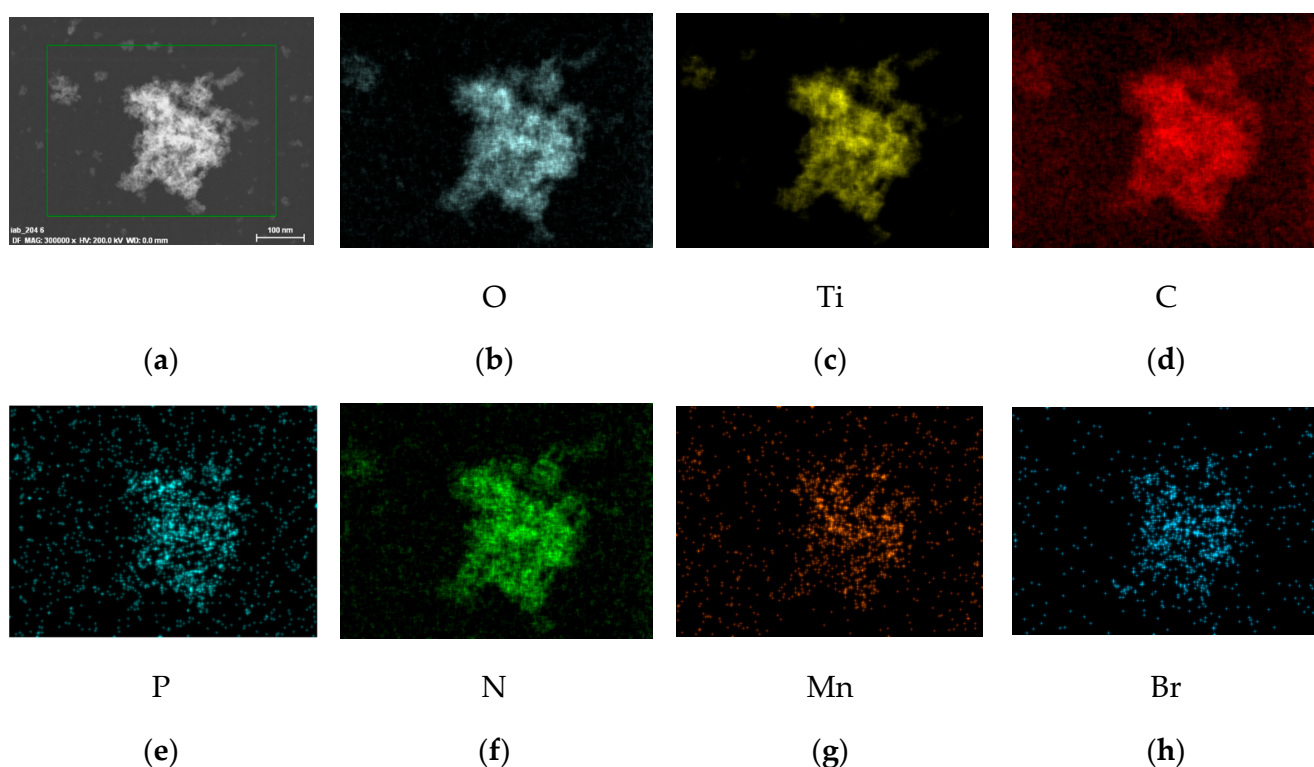
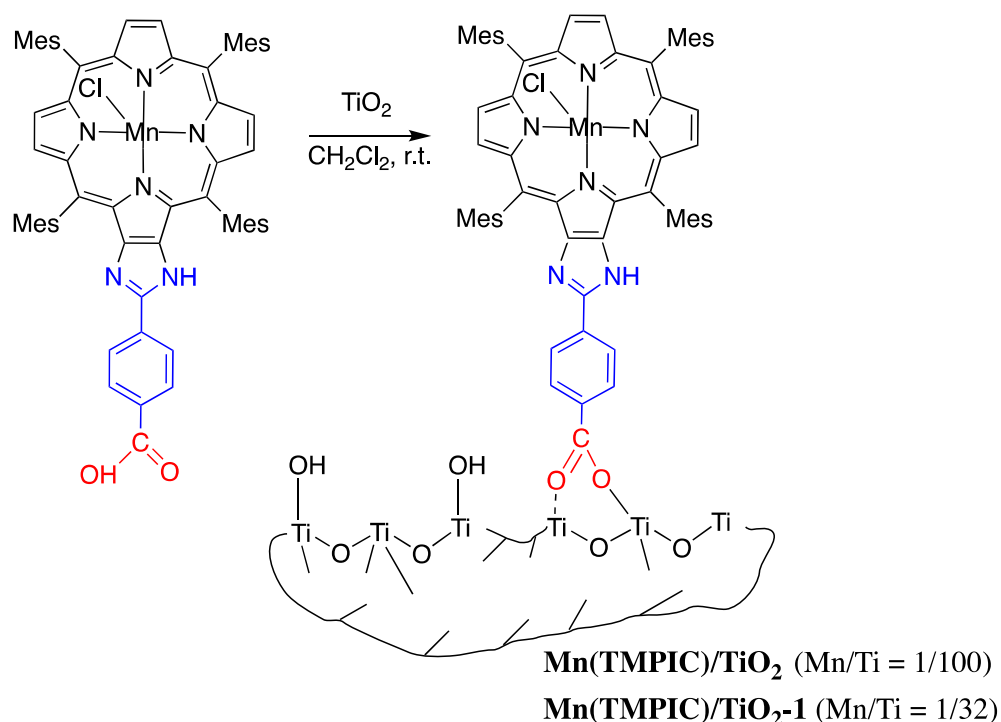


**Figure 3.** STEM image of  $\text{Mn}(\text{TMPIP})/\text{TiO}_2$  before the analysis (a) and EDS elemental mapping images of  $\text{Mn}(\text{TMPIP})/\text{TiO}_2$  (b–h): O (b), Ti (c), C (d), P (e), N (f), Mn (g), Br (h). The acquisition time, i.e., exposure to the electron beam, was 1 h.

The empirical formulas of materials thus obtained were derived from the content of six elements (C, H, N, Ti, Mn and P; see Supplementary Materials, Table S1). The Mn/Ti ratio in the materials  $\text{Mn}(\text{TMPIP})/\text{TiO}_2$  and  $\text{Mn}(\text{TMPIP})/\text{TiO}_2\text{-1}$  was found to be 1:125 and 1:28, respectively. Thus, the content of heterogenized  $\text{Mn}(\text{TMPIP})$  was lower than the expected values in both cases despite the fact that colored filtrates were obtained only during the synthesis of  $\text{Mn}(\text{TMPIP})/\text{TiO}_2\text{-1}$ . To prove quantitative immobilization of  $\text{Mn}(\text{TMPIP})$  onto the solid  $\text{Mn}(\text{TMPIP})/\text{TiO}_2$ , the combined organic and aqueous filtrates obtained during washing the solid were evaporated and dried under reduced pressure. The residue thus obtained was dissolved in methanol and analyzed by UV-vis spectroscopy to check the presence of starting complex  $\text{Mn}(\text{TMPIP})$  and corresponding phosphonic

acid **Mn(TMPIP-OH)**. These two compounds are the only porphyrin products that can be present in the solution if grafting is incomplete. To perform the qualitative analysis, complex **Mn(TMPIP-OH)** was prepared, as shown in Scheme 2. Based on the results of this UV-vis study, we safely concluded that more than 98% of complex **Mn(TMPIP)** was immobilized on a titania support. In contrast, the filtrates were intensively colored when **Mn(TMPIP)** and titania were reacted in a 1:15 molar ratio, and the experimental content of Mn in the target solid was about twice lower than was expected. This likely indicates that maximal catalyst loading (~1:30) was achieved under these experimental conditions.

To enable the immobilization of **Mn(TMPIC)**, the complex was dissolved in dry  $\text{CH}_2\text{Cl}_2$ , and this solution was added to mesoporous titania suspended in the same solvent and stirred for 2 d at room temperature (Scheme 3).



**Scheme 3.** Preparation of materials  $\text{Mn(TMPIC)/TiO}_2$  and  $\text{Mn(TMPIC)/TiO}_2\text{-1}$ .

The Mn/Ti molar ratio also varied between 1:100 and 1:15 for comparative reasons. The empirical formulas of  $\text{Mn(TMPIC)/TiO}_2$  and  $\text{Mn(TMPIC)/TiO}_2\text{-1}$  thus obtained were derived from the content of five elements (C, H, N, Ti and Mn) and were very similar to those of materials based on **Mn(TMPIP)** (Table S1). Quantitative immobilization was observed when complex and inorganic support were reacted in the ratio of 1:100, and the maximal catalyst loading was about 1:32.

The intact structure of the heterogenized complexes **Mn(TMPIP)** and **Mn(TMPIC)** was confirmed by UV-vis diffuse reflectance and FTIR spectroscopies. In brief, the spectral signatures of both manganese complexes before and after immobilization on  $\text{TiO}_2$  were remarkably similar except for the characteristic vibration bands of carboxylic and phosphonic anchors. Kubelka–Munk transformed UV-vis diffuse reflectance spectra of the studied solids show a strong and broad absorption feature in the high energy region (<300 nm). This band was attributed to the  $\text{TiO}_2$  phase. The spectral shape of materials in the 350–750 nm region resembles closely to those observed for **Mn(TMPIC)** and **Mn(TMPIP)** complexes, confirming that the metalloporphyrin residue keeps its integrity after immobilization (Figure 4).



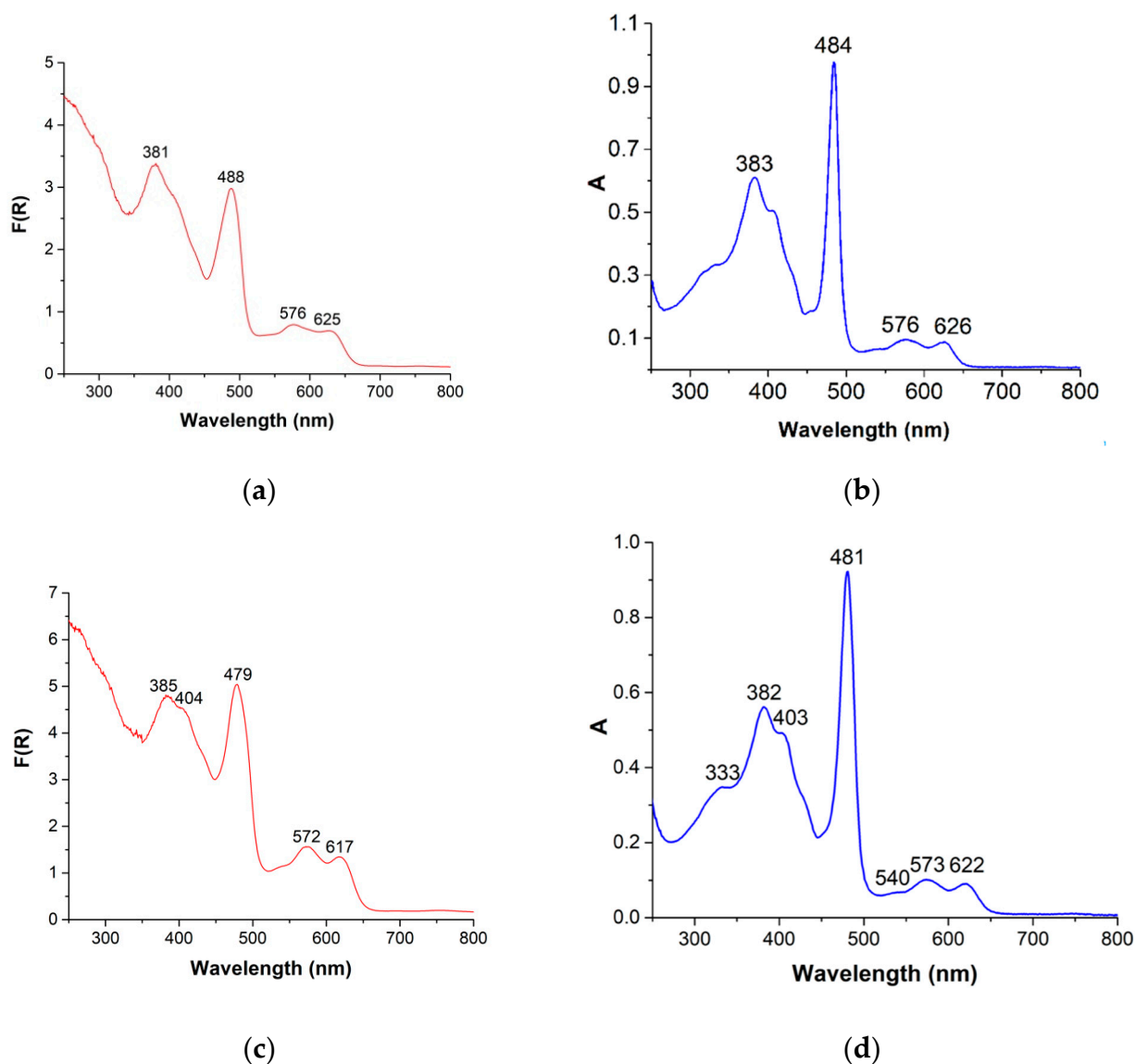


**Figure 4.** Kubelka-Munk transformed diffusion reflectance spectra of **Mn(TMPIP)/TiO<sub>2</sub>-1** (a) and **Mn(TMPIC)/TiO<sub>2</sub>-1** (c). UV-vis spectra of **Mn(TMPIP)** (b) and **Mn(TMPIC)** (d) in chloroform.

In the FTIR spectra (see Supplementary Materials, Figures S6 and S7), vibration bands assigned to the porphyrin macrocycle (720–850 and 1000–1200  $\text{cm}^{-1}$ ) and aryl residues (1350–1610  $\text{cm}^{-1}$ ) are all much weaker as compared to the Ti–OH and O–H stretching modes (3500–3700  $\text{cm}^{-1}$ ) even in the spectra of **Mn(TMPIP)/TiO<sub>2</sub>-1** and **Mn(TMPIC)/TiO<sub>2</sub>-1** materials with high Mn/Ti ratios. Notably, the shape of **Mn(TMPIP)/TiO<sub>2</sub>-1** spectrum in the region of 850–1260  $\text{cm}^{-1}$ , where characteristic bands associated with vibrations of the phosphonate substituent are observed, is significantly different from those of diethoxyphosphoryl-substituted complex **Mn(TMPIP)** and phosphonic acid **Mn(TMPIP-OH)**. Valence vibration bands of P=O residue of the diethoxyphosphoryl group (1250 and 1277  $\text{cm}^{-1}$ ) and of P–O–H of phosphonic acid (916  $\text{cm}^{-1}$ ) are absent. This likely reveals the formation of metal–O–P bonds whose stretching vibrations are overlapped with those of the porphyrin macrocycle, giving a rather strong band at 1003  $\text{cm}^{-1}$ . In the spectrum of **Mn(TMPIC)/TiO<sub>2</sub>-1**, stretching vibrations of the carboxylic acid group (1719  $\text{cm}^{-1}$  for **Mn(TMPIC)**) were not observed, pointing out the involvement of this anchoring group in the interaction with the titania support.

The morphology of **Mn(TMPIP)/TiO<sub>2</sub>** was studied by SEM and compared to that of the bare TiO<sub>2</sub> (Figures 5 and S8). The latter is composed of strongly aggregated nanoparticles of similar shape and narrow grain-size distribution. The incorporation of **Mn(TMPIP)** does not have any influence on the cauliflower-like morphology of the solid. The mesoporous nanospheroids, with diameters ranging from 5 to 20 nm, are irregularly distributed in space and separated by large holes of hundreds of nanometers, thus providing good accessibility to the bound complexes of catalytic sites. This morphology is, therefore, perfectly suited for application of the material in catalysis.

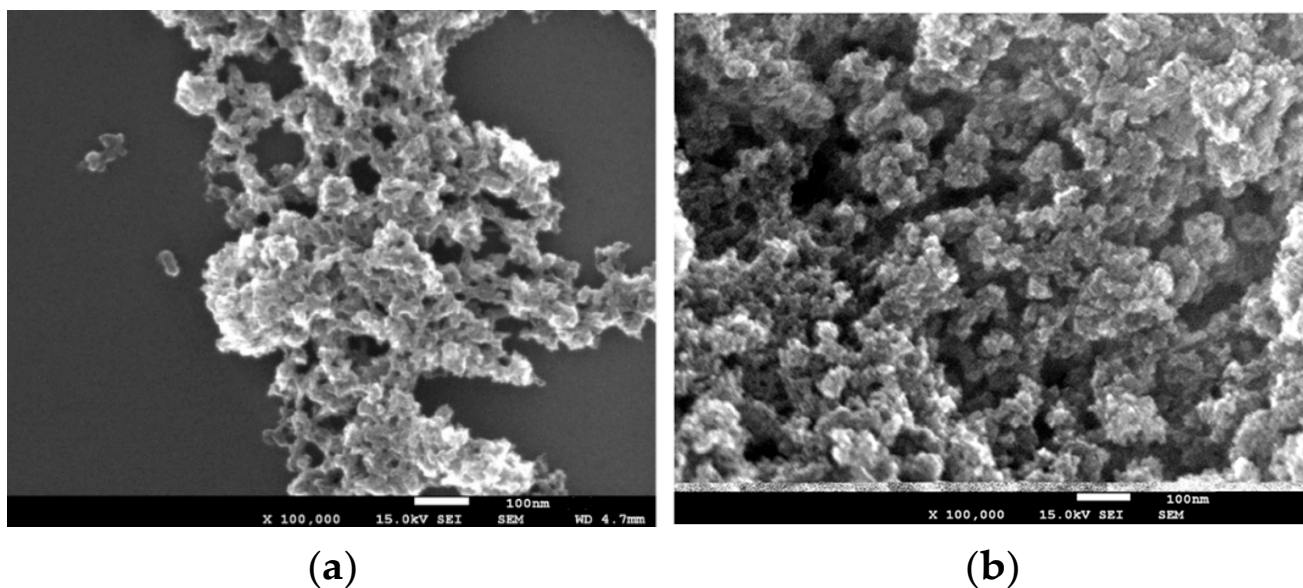


**Figure 5.** SEM microphotographs of (a) bare hydrated TiO<sub>2</sub> and (b) **Mn(TMPIP)/TiO<sub>2</sub>**.

N<sub>2</sub> adsorption-desorption isotherms of all four hybrid materials were recorded at 77 K, and the results of these analyses were summarized in Table S2 (see Supplementary Materials). Upon the derivatization of TiO<sub>2</sub>, no change in the shape of the isotherms was observed, whereas a marked decrease in the BET surface area and volume of pores for all samples was noted, which was consistent with the presence of grafted complexes in the mesopores. It's worth noting that materials **Mn(TMPIP)/TiO<sub>2</sub>-1** and **Mn(TMPIC)/TiO<sub>2</sub>-1** with high porphyrin loading display smaller BET surface areas and pore volumes as compared to their counterparts **Mn(TMPIP)/TiO<sub>2</sub>** and **Mn(TMPIP)/TiO<sub>2</sub>** charged less in porphyrin complexes. These data agree well with the hypothesis that both complexes are located not only at the outside titania surface but also in its mesopores.

Powder X-ray diffraction measurements confirmed that the pristine mesoporous titania and all samples of functionalized materials prepared in this work are amorphous solids.

The materials with high catalysts loading **Mn(TMPIP)/TiO<sub>2</sub>-1** and **Mn(TMPIC)/TiO<sub>2</sub>-1** were chosen for comparative studies of their stability in different organic solvents and in aqueous media with variable pH. A suspension of the solid in toluene, chlorinated (CH<sub>2</sub>Cl<sub>2</sub>, CHCl<sub>3</sub>), polar (CH<sub>3</sub>CN, DMF), and protic (MeOH, EtOH) solvents were centrifugated after 1 week, and the solutions thus obtained were analyzed visually or using a laboratory spectrophotometer. Only **Mn(TMPIP)/TiO<sub>2</sub>-1** with the phosphonate anchor was stable in all these solvents, which is commonly used in organic synthesis. **Mn(TMPIC)/TiO<sub>2</sub>-1** was rapidly washed off in protic solvents (>50%) and also in acetonitrile (~10%).

The stability of **Mn(TMPIP)/TiO<sub>2</sub>-1** was also explored in aqueous media in all pH ranges. The leaching of the complex was observed only in basic solutions (pH > 9). We also found that **Mn(TMPIP)/TiO<sub>2</sub>-1** was stable in the presence of triethylamine in CHCl<sub>3</sub> and DMF. This is important for organic synthesis because tertiary amines are common reagents in catalytic and photocatalytic transformations.

The more stable heterogenized complex with spatially separated catalytic sites (**Mn(TMPIP)/TiO<sub>2</sub>**) was next studied as a catalyst in oxidation reactions.

### 2.3. Catalytic Reactions

To get insight into the catalytic properties of **Mn(TMPIP)/TiO<sub>2</sub>**, we studied its catalytic efficiency and reusability in the oxidation reactions using molecular oxygen as a terminal oxidant and isobutyraldehyde (IBA) as a sacrificial reagent (Mukaiyama conditions [80]) because these mild oxidation conditions are suitable for transformations of different compounds such as alkanes, alkenes, aldehydes, cyclic ketones, sulfides and alcohols [81–85]. Metalloporphyrins are known as active catalysts for these reactions under homogeneous conditions [12,16,81,83,86,87]. In our work, the oxidation of sulfide to sulfoxide was chosen as a model reaction. Selective sulfoxidation attracts considerable interest due to its relevance to biochemistry, warfare agent disposal, the environmental consequences of fuel desulfurization, and organic synthesis [88–95]. The overoxidation of sulfides to sulfones and the cleavage of S–C and (S)C–H bonds are commonly observed as side reactions [96–98], and thus selective methods for transformation of different sulfides are in high demand, in particular in the asymmetric synthesis of ligands and in the development of pharmaceuticals involving selective late-stage oxygenation [93,95,99–101].

In the preliminary experiments, the oxidation of thioanisole with molecular oxygen (1 atm) was performed in the presence of 0.09 mol% of TiO<sub>2</sub>-supported complex **Mn(TMPIP)** and 6 equivalents of IBA in toluene at 80 °C and monitored by GC-MS (Table 1). Starting sulfide was consumed in less than 30 min, but the overoxidation of sulfoxide to methyl phenyl sulfone (42%) was observed as a side reaction (entry 1). To diminish the overoxidation, the temperature was decreased to 40 °C (entry 2). Under these conditions, the reaction proceeded more slowly, but sulfone was obtained in a similar yield (37%). Comparing the amount of sulfone in the reaction mixture before and after complete consumption of sulfide in the reaction performed at 30 °C (entry 3), we concluded that the overoxidation was slow until the starting sulfide was present in the reaction mixture but was significantly accelerated after the sulfide consumption. The results obtained at 20 °C confirmed this hypothesis, but the control of the overoxidation was difficult, even under these mild conditions, because the reaction was too rapid (entry 4). Thus, the amount of IBA was decreased up to three equivalents. The rate of oxidation was decreased, and methyl phenyl sulfoxide was the main product (96%) when 76% of starting sulfide was consumed (entry 5). However, when this reaction was prolonged for additional 2 h, only 10% of starting sulfide was reacted, probably due to the complete consumption of IBA. Oxidation at 50 °C also gave only sulfoxide when 52% of sulfide was reacted (entry 6), but 6% of starting compound was still observed after 8 h of reacting. Finally, adjusting the amount of IBA to reach a complete conversion and an appropriate reaction rate (5 equivalents), the sulfoxide was obtained in about quantitative yield (entry 7).

It is noteworthy that the oxidation did not proceed at all in the absence of **Mn(TMPIP)/TiO<sub>2</sub>**, IBA, or oxygen under these conditions (entries 8–10). Our attempts to use non-functionalized TiO<sub>2</sub> as a catalyst (entry 11) or to decrease catalyst loading 10 times (entry 12) failed.

Thus, as low as 0.09 mol% of TiO<sub>2</sub>-supported **Mn(TMPIP)** were required for the selective sulfoxidation of thioanisole with molecular oxygen in the presence of five equivalents of IBA (TON = ~1100, TOF = ~370 h<sup>-1</sup>) in a single catalytic run of the sulfoxidation of thioanisole. The overoxidation of sulfide to sulfone in the presence of this catalyst proceeds even at room temperature, but sulfoxides can be obtained in a quantitative yield controlling the amount of IBA, temperature, and the time of reacting.

**Table 1.** Oxidation of thioanisole by molecular oxygen in the presence of Mn(TMPIP)/TiO<sub>2</sub> and IBA<sup>1</sup>.

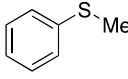
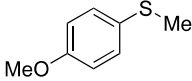
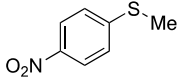
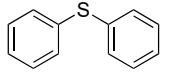
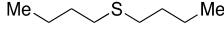
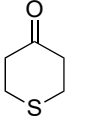
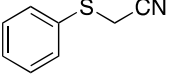
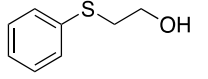
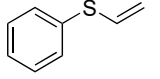
Entry	IBA (Equiv.)	Temperature (°C)	Time (h)	Conversion <sup>2</sup> (%)	Selectivity <sup>2</sup> (%)	
					Sulfoxide	Sulfone
1	6	80	0.5	100	58	42
2	6	40	2	100	63	37
3	6	30	2.5	92	99	1
			3	100	53	47
4	6	20	2	85	100	0
			2.5	100	82	12
5	3	80	1.5	76	96	4
			3.5	86	86	14
6	3	50	1.5	52	100	0
			8	94	95	5
7	5	20	3	100	98	2
8 <sup>3</sup>	5	20	3	0		
9	0	20	3	0		
10 <sup>4</sup>	5	20	3	0		
11 <sup>5</sup>	5	20	3	0		
12 <sup>6</sup>	5	20	3	0		

<sup>1</sup> Reaction conditions: 2.5 mmol of thioanisole, molecular oxygen (1 atm), IBA, 0.09 mol% of heterogenized Mn(III) porphyrin (based on the formula of Mn(TMPIP)/TiO<sub>2</sub>, which was calculated from the data of elemental analysis and ICP-OES (Table S1)), toluene (10 mL) were stirred at a given temperature. <sup>2</sup> Conversion and selectivity were determined by GC-MS analysis of reaction mixtures. Naphthalene was used as an internal standard. <sup>3</sup> The reaction was performed without a transition metal catalyst. <sup>4</sup> The experiment was performed in Ar (1 atm). <sup>5</sup> The catalyst was replaced by bare TiO<sub>2</sub>. <sup>6</sup> The reaction was carried out in the presence of 0.009 mol% of the heterogenized complex.

To determine whether the catalyst leaching was observed under reaction conditions and show that the reaction was not catalyzed by the non-supported manganese complex in solution, a “hot filtration test” was performed (see Supplementary Materials, Figure S9). Half of the solution was filtered when 50% of the starting sulfide was consumed, and both reactions were continued under identical conditions. In the filtered solution, oxidation was also observed but was much slower than in the suspension. To prove the absence of catalyst leaching, we determined the content of manganese-containing compounds in the residue obtained after evaporation of the homogeneous reaction mixture using the ICP-OES technique. The manganese content was found to be less than 5 ppm. Based on these data, we assumed that the oxidation reaction observed in the filtrated solution proceeds without the participation of transition metal catalysts. This can be the sluggish autoxidation of sulfides in the presence of O<sub>2</sub> and IBA, as reported previously [102,103].

Encouraged by these results, we investigated the scope of substrates for this reaction. To our surprise, various sulfides can be selectively oxidized to sulfoxides under ambient conditions controlling the amount of IBA introduced into the reaction (Table 2). The rate of oxidation of aryl methyl sulfides is dependent on the nature of substituents on the phenyl ring. Electron-rich derivatives are more reactive than compounds with electron-deficient aryl groups. For instance, 4-methoxythioanisole was converted to sulfoxide in 2 h, but the reaction time should be prolonged to 7 h if 4-nitrothioanisole was oxidized. Nevertheless, all target products were obtained in almost quantitative yield. The oxidation of more sterically hindered diphenyl sulfide, which is known to be resistant to oxidation by O<sub>2</sub> under photocatalytic conditions [104], can be performed with excellent selectivity using only 3.3 equivalents of IBA and 6 h of reacting under otherwise identical conditions to give the target product in a 92% yield.

**Table 2.** Oxidation of sulfides by molecular oxygen in the presence of Mn(TMPIP)/TiO<sub>2</sub> and IBA <sup>1</sup>.

$R_1-S-R_2 \xrightarrow[O_2, IBA, \text{toluene}]{0.09 \text{ mol\% Mn(TMPIP)/TiO}_2} R_1-S(=O)-R_2 + R_1-S(=O)_2-R_2$						
Entry	Sulfide	IBA (Equiv.)	Time (h)	Conversion <sup>2</sup> (%)	Selectivity <sup>2</sup> (%)	
					Sulfoxide	Sulfone
1		5	2.5	100	98	2
2		5	2	100	98	2
3		5	7	100	97	3
4		3.3	6	100	92	8
5		6	4	94	98	2
6		9	2.5	92	92	8
7		3	3	99	94	6
8		10	4	98	97	3
9		7	4	98	89	11

<sup>1</sup> Reaction conditions: 2.5 mmol of thioanisole, IBA, 0.09 mol% of heterogenized complex (calculations were based on the data of ICP analysis of Mn(TMPIP)/TiO<sub>2</sub>), toluene (10 mL) were stirred at a given temperature under molecular oxygen (1 atm). <sup>2</sup> Conversion and selectivity were determined by GC-MS analysis of reaction mixtures. Naphthalene was used as an internal standard.

Linear and cyclic dialkyl sulfides were found to be less reactive than aryl sulfides and were oxidized in the presence of 6–9 equivalents of IBA. The oxidation of cyclic derivative seems to be less selective because sulfoxide and sulfone were obtained in a 92:8 ratio when only 92% of the sulfide was consumed.

Finally, we explored the sulfoxidation of compounds bearing additional oxidizable sites such as vinyl, hydroxyl and cyano substituents (entries 7–9). To our great satisfaction, all target sulfoxides were obtained in a high yield, and the overoxidation of sulfoxide was only observed as a side reaction. Despite the reactions being optimized only briefly, even in the case of the most problematic phenyl vinyl sulfide, the sulfoxide:sulfone ratio was 89:11 when 90% of starting compound was consumed.

The mechanistic pathways of oxidation by the O<sub>2</sub>-IBA reagent system were debated in the literature [12,105–109]. Several active species with and without transition metal atoms were identified. The relative efficacy by which a sulfide molecule is oxidized by one versus the other pathways appears to be dependent on the nature of the transition metal catalyst, solvent and temperature. Despite mechanistic studies of porphyrin catalysts being very limited, high-valent metalloporphyrin-oxo intermediates were considered as main active oxygen-containing intermediates [108,110–112]. Our data do not contradict this hypothesis because the oxidation is more rapid in the presence of the Mn(III) complex, as was shown in

the “hot filtration test.” However, other less-active oxygen-containing intermediate species can also contribute to the formation of the target product. Detailed mechanistic studies of this reaction are beyond the scope of this work.

Catalyst recovery and refining were straightforward. After completion of the reaction, the catalyst was isolated by centrifugation, washed with toluene and introduced in the next cycle. Seven consecutive oxidation reactions of thioanisole were carried out, giving the target sulfoxides in comparable yields (94–98%; Figure 6 and Table S3 (see Supplementary Materials)). The reaction time was different in these experiments, but the changes were non-systematic, probably because this reaction parameter is highly dependent on the efficiency of stirring heterogeneous reaction mixtures. The content of resting manganese derivatives in the crude products was found to be less than 5 ppm by using the ICP-OES analysis (Table S3 (see Supplementary Materials)). This proves that catalyst leaching in the reaction mixture was negligible. The integrity of the  $\text{Mn}(\text{TMPIP})/\text{TiO}_2$  catalyst was also confirmed by studying the solid recovered after the last catalytic cycle by diffuse reflectance spectroscopy. As shown in Figure S10 (see Supplementary Materials), the solid exhibits absorption features characteristic of  $\text{Mn}(\text{TMPIP})$  in  $\text{CHCl}_3$  solution and  $\text{Mn}(\text{TMPIP})/\text{TiO}_2$  material. A small bathochromic shift of spectral band positions was observed for several bands in the spectrum of the recovered solid. This likely indicates a difference in the adsorbed solvent molecules in the starting and reused catalysts or the chemical modification of the  $\text{TiO}_2$  surface (the esterification by isobutyric acid, for instance) during the oxidation reaction. Nevertheless, based on these spectral data, we can safely conclude that the heterogenized porphyrin macrocycle is not decomposed after seven consecutive oxidation cycles.

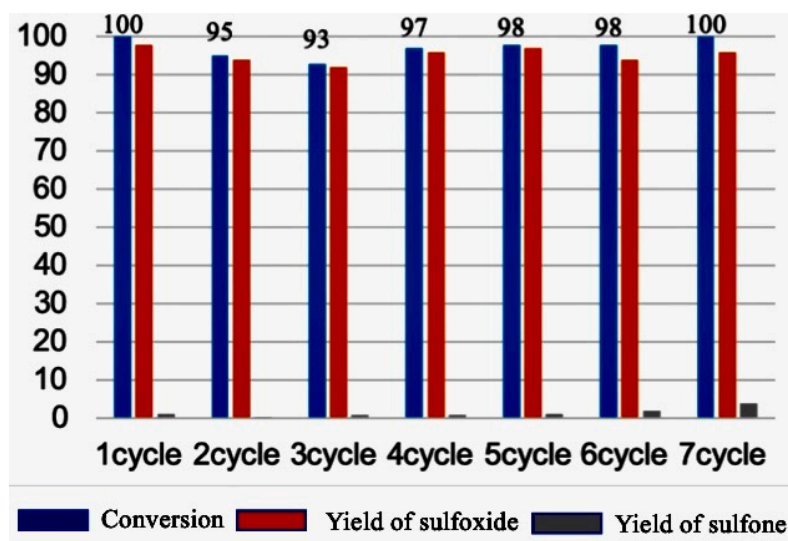


Figure 6. Recycling of  $\text{Mn}(\text{TMPIP})/\text{TiO}_2$  in the oxidation of thioanisole by  $\text{O}_2$  in the presence of IBA.

When oxidation of thioanisole was performed under homogeneous conditions replacing  $\text{Mn}(\text{TMPIP})/\text{TiO}_2$  by its soluble counterpart  $\text{Mn}(\text{TMPIP})$  or commercially available (*meso*-tetramesitylporphyrinato)manganese(III) chloride ( $\text{Mn}(\text{TMP})$ ) only starting thioanisole was observed in the reaction mixture after 24 h of reacting. When  $\text{Mn}(\text{TMPIP})$  loading was increased up to 0.5 mol%, only 15% of thioanisole was converted to sulfoxide after 24 h. Thus, immobilization of  $\text{Mn}(\text{TMPIP})$  on hydrated titania significantly increases its catalytic efficiency allowing us to perform sulfoxidation under ambient conditions. The reason for the synergetic effect is unclear at this point of investigation. We cannot exclude that the adsorption of sulfides on a large surface of inorganic support accelerates the oxidation reaction, but most probably, peroxide intermediates formed on the surface of hydrated  $\text{TiO}_2$  [113] also participated in the oxidation.

Comparing **Mn(TMPIP)/TiO<sub>2</sub>** with porphyrin catalysts reported previously, we can conclude that this material is situated among the best catalysts known for the sulfoxidation reaction. Indeed, the oxidation of sulfides by sodium periodate in the presence of Mn(III) porphyrins grafted on polystyrene [114] or silica [115] led to a mixture of sulfoxides and sulfones. When Mn(III) porphyrins were grafted on graphene oxide and used as catalysts for the sulfoxidation by hydrogen peroxide-urea adduct, about 2 mol% of catalysts were required, and the reactions were less selective, in particular when aromatic sulfides were used as substrates [116]. Fe(III) porphyrins grafted on activated multi-walled carbon nanotubes were efficient in ethanol when tetra-*n*-butylammonium peroxomonosulfate was used as an oxidant, but some of the studied reactions were difficult to control [117]. Several heterogenized porphyrin catalysts were also reported for the oxidation of sulfides to sulfoxides under Mukaiyama conditions. Manganese(III) complex with 5,10,15,20-tetrakis(*N*-methylpyridinium-4-yl)porphyrin immobilized in montmorillonite gave the selective transformation only when the reaction was conducted at 50–80 °C [34]. Only COP based on Fe(III) porphyrin has shown catalytic activity similar to that of **Mn(TMPIP)/TiO<sub>2</sub>** [45]. However, this immobilization procedure requires a large amount of the complex and yields hybrid materials in which the number of catalytic sites cannot be optimized.

It's also worth noting that porphyrin catalysts bearing phosphonate anchors were successfully immobilized onto the zinc phosphonate network with low porosity [118] and incorporated onto zirconium phosphonate film materials [119]. Our immobilization strategy is complementary to these approaches and gave porous porphyrin catalysts.

### 3. Materials and Methods

#### 3.1. General

Unless otherwise noted, all chemicals and starting materials were obtained commercially from Acros (via Thermo Fisher Scientific, Illkirch, France) or Aldrich-Sigma Co. (via Merck Co., Darmstadt, Germany) and used without further purification. (5,10,15,20-Tetramesitylporphyrinato)manganese(III) chloride (**Mn(TMPP)**) was provided by Porphyr-Chem (Dijon, France). 2-Nitro-5,10,15,20-tetramesitylporphyrin was prepared according to the literature protocol [120]. 5,10,15,20-Tetramesityl-2-(4-carboxyphenyl)-1*H*-imidazo[4,5-*b*]porphyrin (**2H(TMPPIC)**) and 5,10,15,20-tetramesityl-2-[4-(diethoxyphosphoryl)phenyl]-1*H*-imidazo[4,5-*b*]porphyrin (**2H(TMPIP)**) were synthesized according to a procedure developed by us previously [58,121]. Mesoporous hydrated titanium(IV) oxide was prepared using a surfactant-free sol-gel procedure reported by us previously [76]. The content of Ti in the solid thus obtained was determined by ICP-OES analysis. Preparative column chromatography was carried out using silica gel 60 (40–63 μm) from Merck Co. (Darmstadt, Germany). CH<sub>2</sub>Cl<sub>2</sub> was distilled over CaH<sub>2</sub>.

UV-vis absorption spectra were collected with an Agilent Cary 60 (Massy, France) using Suprasil 300 cuvettes (Hellma, *l* = 1 cm). Diffuse reflectance spectra of materials were acquired on a Cary 5000 (Massy, France) UV-vis-NIR spectrophotometer outfitted with a praying Mantis<sup>TM</sup> accessory (Harrick, via Agilent, Massy, France). The baseline was recorded with a Spectralon<sup>®</sup> pellet. Corrected reflectance data (*R*) were converted to *f*(*R*) values using the Kubelka–Munk function expressed as  $f(R) = (1 - R^2)/2R$ .

FTIR spectra were registered either on a Nicolet iS 5 (Thermo Fisher Scientific, Illkirch, France) or a Bruker Vector 22 (Wissembourg, France) spectrophotometer. A micro-ATR accessory (Pike) was used in order to obtain FTIR spectra of solid polycrystalline complexes.

MALDI-TOF mass-spectra were obtained on a Bruker Ultraflex II LRF 2000 (Wissembourg, France) mass-spectrometer in positive ion mode with the dithranol matrix. Accurate mass measurements (HRMS-ESI) were performed with a Thermo Scientific Orbitrap Elite high-field Orbitrap hybrid mass spectrometer (Thermo Fisher Scientific, Illkirch, France). The samples were dissolved in a methanol/chloroform (1:1, *v/v*) solvent mixture and analyzed in positive mode. Microanalyses (CHN) were performed using a Thermo Electron Flash EA 1112 analyzer (Thermo Fisher Scientific, Illkirch, France). Mn, P and Ti contents were measured by inductively coupled plasma optical emission spectrometry (ICP-OES

DUO) on an ICAP 7400 instrument from Thermo Fisher Scientific (Illkirch, France). The samples were mineralized using standard procedures.

Field-emission scanning electron microscopy (FESEM) was performed using a JEOL JSM 7600F (JEOL (Europe) SAS, Croissy-sur-Seine, France) instrument located in the ARCEN analysis center of the University of Bourgogne (Dijon, France). Images were acquired using GentleBeam-High SEM mode. Transmission electron microscopy (TEM) analyses were conducted using a JEOL JEM-2100F microscope ((JEOL (Europe) SAS, Croissy-sur-Seine, France) operating at 200 kV and located in the ARCEN analysis center of the University of Bourgogne (Dijon, France). EDX spectroscopy in STEM mode was used for chemical mapping and qualitative and quantitative elemental analysis using a Bruker XFlash Detector 5030 spectrometer fitted on the JEM-2100F microscope (Bruker, Wissembourg, France).

Nitrogen adsorption-desorption isotherms were measured with a BELSORP max analyzer (BEL Japan, INC, via Mercer Instruments, Passy, France) at 77 K with samples degassed for 6 h at 80 °C under reduced pressure ( $10^{-5}$  torr). Specific surface areas ( $S_{\text{BET}}$ ) were calculated according to the Brunauer–Emmett–Teller (BET) method.

Powder X-ray diffraction experiments were performed with an Empyrean diffractometer from the PANalytical company (Palaiseau, France) in the range  $3^\circ < 2\theta < 50^\circ$ , using a copper anticathode X-ray tube ( $\text{Cu K}\alpha_1 = 1.54060 \text{ \AA}$  and  $\text{Cu K}\alpha_2 = 1.54443 \text{ \AA}$ ) and an X'Celerator detector outfitted with an anti-scattering slit of 5 mm. The uncrushed samples were placed between 2 Mylar sheets, and the analysis was carried out in transmission mode using a focusing X-ray mirror equipped with fixed divergent and anti-scattering slits (aperture  $0.5^\circ$ ) and 0.02 rad Soller slits.

All elemental analyses except EDX analyses were performed at the “Pôle Chimie Moléculaire,” the technological platform for chemical analysis and molecular synthesis (<http://www.wpcm.fr>, accessed on 30 December 2022) of the Institut de Chimie Moléculaire de l'Université de Bourgogne and Welience<sup>TM</sup>, a private subsidiary of the Université de Bourgogne.

### 3.2. Synthesis of Manganese(III) Complexes *Mn*(TMPIC), *Mn*(TMPIP) and *Mn*(TMPIP-OH)

*General procedure.* To a solution of free base porphyrin (0.1 mmol) in dimethylformamide (13 mL), manganese dichloride (63 mg, 0.5 mmol, 5 equivalents) was added at 150 °C. The reaction mixture was stirred at this temperature and monitored by TLC. After complete consumption of starting porphyrin (4 h), the reaction mixture was cooled to room temperature and evaporated under reduced pressure. The residue thus obtained was dissolved in dichloromethane (30 mL), and the solution was washed with water ( $3 \times 20$  mL), dried over  $\text{MgSO}_4$  and evaporated under reduced pressure. The residue thus obtained was chromatographed on silica gel using  $\text{CH}_2\text{Cl}_2/\text{MeOH}$  as eluent.

[5,10,15,20-tetramesityl-2-(4-carboxyphenyl)-1H-imidazo[4,5-b]porphyrinato]manganese(III) chloride (**Mn**(TMPIC)). The complex was prepared according to the general procedure from **2H**(TMPIC) (120 mg, 0.127 mmol) and isolated as a green solid using  $\text{CH}_2\text{Cl}_2/\text{MeOH}$  (95:5 v/v) as an eluent. Yield 92% (116 mg); mp > 320 °C, decomp. UV-vis ( $\text{CHCl}_3$ ,  $\lambda_{\text{max}}$ , nm ( $\log(\epsilon \text{ (cm}^{-1}\text{M}^{-1}))$ ): 333 (4.60), 382 (4.80), 403 (4.75), 481 (5.00), 540 (sh), 573 (4.09), 622 (4.04), and 748 (3.04). FTIR (neat,  $\nu$ ,  $\text{cm}^{-1}$ ): 3410 (w, NH), 2913 (m), 2849 (m), 1719 (m, C=O), 1610 (m), 1437 (w), 1378 (w), 1331 (w), 1250 (w), 1225 (w), 1195 (m), 1003 (s), 862 (w), 851 (w), 833 (m), 802 (m), and 721 (m). HRMS-ESI:  $m/z$   $[\text{M}-\text{Cl}]^+$  calcd for  $\text{C}_{64}\text{H}_{56}\text{MnN}_6\text{O}_2$ : 995.38398; found: 995.38814.

[5,10,15,20-tetramesityl-2-[4-(diethoxyphosphoryl)phenyl]-1H-imidazo[4,5-b]porphyrinato]manganese(III) chloride (**Mn**(TMPIP)). The complex was prepared according to the general procedure from **2H**(TMPIP) (554 mg, 0.535 mmol) and isolated as a green solid using  $\text{CH}_2\text{Cl}_2/\text{MeOH}$  (95:5 v/v) as eluent. Yield 60% (330 mg); mp > 320 °C, decomp. UV-vis ( $\text{CHCl}_3$ ,  $\lambda_{\text{max}}$ , nm ( $\log(\epsilon \text{ (cm}^{-1}\text{M}^{-1}))$ ): 327 (4.46), 383 (4.72), 407 (4.65), 484 (4.92), 576 (3.93), 626 (3.89), and 749 (2.92). FTIR (neat,  $\nu$ ,  $\text{cm}^{-1}$ ): 3385 (w, NH), 2916 (w), 2854 (w), 1609 (w), 1475 (w), 1437 (w), 1410 (w), 1377 (w), 1333 (w), 1248 (m, P=O), 1227 (m, P=O), 1196 (m),



1130 (m), 1051 (m), 1016 (s, P–O–C), 1003 (s), 953 (m), 851 (w), 833 (m), 800 (s), 762 (w), 719 (m), and 665 (w). HRMS-ESI:  $m/z$  [M-Cl+H]<sup>2+</sup> calcd for C<sub>67</sub>H<sub>66</sub>MnN<sub>6</sub>O<sub>3</sub>P: 544.21518; found: 544.21526; [M-Cl]<sup>+</sup> calcd for C<sub>67</sub>H<sub>65</sub>MnN<sub>6</sub>O<sub>3</sub>P: 1087.42308; found: 1087.42690; [M+H]<sup>+</sup> calcd for C<sub>67</sub>H<sub>66</sub>ClMnN<sub>6</sub>O<sub>3</sub>P: 1123.39976; found: 1123.39579.

[5,10,15,20-tetramesityl-2-[4-(dihydroxyphosphoryl)phenyl]-1H-imidazo[4,5-b]porphyrin-ato] manganese(III) bromide (**Mn(TMPIP-OH)**).

A dry Schlenk tube was charged with diethyl phosphonate ester **Mn(TMPIP)** (15 mg, 0.0134 mmol) and dry CH<sub>2</sub>Cl<sub>2</sub> (5 mL) under argon. Then, TMSBr (53 mL, 0.4 mmol, 30 equivalents) was added via a syringe, and the resulting mixture was stirred for 3 d at r. t. and monitored by MALDI-TOF mass spectrometry. After the complete consumption of ethyl phosphoesters, methanol (2 mL) was added to the reaction mixture, and stirring was continued for 30 min. Evaporation of volatiles under reduced pressure afforded the target phosphonic acid as a dark green solid. Yield: 90% (14 mg); mp > 350 °C, decomp. UV-vis (CHCl<sub>3</sub>, λ<sub>max</sub>, nm (log(ε (cm<sup>-1</sup>M<sup>-1</sup>)))): 303 (4.40), 385 (4.78), 419 (4.73), 452 (4.53), 491 (4.81), 587 (3.90), 633 (3.92), and 760 (2.86). FTIR (neat, ν, cm<sup>-1</sup>): 2918 (m), 2853 (m), 1609 (w), 1437 (m), 1408 (w), 1379 (w), 1335 (w), 1196 (m), 1134 (w), 1003 (s), 916 (m, P–OH), 851 (w), 831 (s), 802 (s), 719 (s), and 663 (w). HRMS-ESI:  $m/z$  [M-Br]<sup>+</sup> calcd for C<sub>63</sub>H<sub>57</sub>MnN<sub>6</sub>O<sub>3</sub>P: 1031.36048; found: 1031.36328; [M-HBr+Na]<sup>+</sup> calcd for C<sub>63</sub>H<sub>56</sub>MnN<sub>6</sub>NaO<sub>3</sub>P: 1053.34242; found: 1053.34345. HRMS-ESI spectrum is shown in Figure S4.

### 3.3. Synthesis of Heterogenized Catalysts

**Grafting complex Mn(TMPLIC).** A dry Schlenk tube was charged with carboxylic acid **Mn(TMPLIC)** (18 mg, 0.018 mmol) and dry CH<sub>2</sub>Cl<sub>2</sub> (50 mL) under argon. Then mesoporous hydrated TiO<sub>2</sub> (18 mmol, 100 equivalents) was added under an argon stream. The suspension was stirred for 2 d at r.t. The solid was collected by centrifugation and thoroughly washed with THF (2 × 20 mL), water (15 mL), MeOH (3 × 15 mL), and ether (2 × 15 mL). The material was finally dried for 24 h at 80 °C under reduced pressure (2 mmHg). Yield: 165 mg.

The solid **Mn(TMPLIC)/TiO<sub>2</sub>-1** with a high content of **Mn(TMPLIC)** (the **Mn(TMPLIC)**:TiO<sub>2</sub> ratio was 1:15) was also prepared according to this procedure.

**Grafting complex Mn(TMPIP).** A dry Schlenk tube was charged with diethyl phosphonate ester **Mn(TMPIP)** (360 mg, 0.32 mmol) and dry CH<sub>2</sub>Cl<sub>2</sub> (50 mL) under argon. Then, TMSBr (30 equiv equivalents) was added via a syringe, and the resulting mixture was stirred for 48 h at r. t. The reaction was monitored by MALDI-TOF mass spectrometry to ensure a complete conversion had occurred before the evaporation of volatiles under reduced pressure. Then, 50 mL of dry CH<sub>2</sub>Cl<sub>2</sub> was introduced into the Schlenk tube with a syringe, followed by the addition of mesoporous hydrated TiO<sub>2</sub> (32 mmol, 100 equivalents) under an argon stream. The suspension was stirred for 2 d at r. t. The solid was collected by centrifugation and thoroughly washed with THF (2 × 20 mL), water (15 mL), MeOH (3 × 15 mL), and ether (2 × 15 mL). The material was dried for 24 h at 80 °C under reduced pressure (2 mmHg). Yield: 3050 mg.

The solid **Mn(TMPIP)/TiO<sub>2</sub>-1** with a high content of **Mn(TMPIP)** (ratio of **Mn(TMPIP)**:TiO<sub>2</sub> was 1:15) was prepared according to this procedure.

### 3.4. Catalytic Reactions

**General procedure.** A 25 mL two-necked flask equipped with a magnetic stir bar and a back-flow condenser was charged with 0.09 mol% of heterogenized **Mn(TMPIP)** (calculations were based on the data of ICP-OES analysis of **Mn(TMPIP)/TiO<sub>2</sub>**, Table S1). The reaction vessel was evacuated and purged by oxygen 3 times. Subsequently, 2.5 mmol of sulfide, the calculated amount of IBA (Tables 1 and 2), and 10 mL of toluene were added by syringe, and the reaction mixture was stirred under oxygen (filled balloon), controlling the temperature (see Tables 1 and 2). The reaction was periodically monitored by GC-MS, and quantitative analyses were performed using naphthalene as an internal standard. When the reaction was complete, the mixture was centrifugated, and the filtrate

was washed with water ( $3 \times 5$  mL), dried over  $\text{MgSO}_4$  and evaporated under reduced pressure at room temperature. The structure of the target product was confirmed by  $^1\text{H}$  NMR, comparing its spectral data with those reported previously in the literature.

Turnover number (TON = Number of product molecules/Number of active catalytic sites) and turnover frequency (TON in an hour) were estimated using a calculated value of catalyst loading (0.09 mol%).

In the experiment with bare  $\text{TiO}_2$  (Table 1, entry 11), the amount of hydrated titania was identical to that which was used in the experiments with  $\text{Mn}(\text{TMPIP})/\text{TiO}_2$ . The calculations were performed using the empirical formula obtained from the data of elemental analysis and ICP-OES.

*Methyl phenyl sulfoxide* (Table 2, entry 1) [122].  $^1\text{H}$  NMR ( $\text{CDCl}_3$ , 400 MHz): 2.72 (s, 3H,  $\text{CH}_3$ ), 7.50–7.58 (m, 3H, Ar), 7.63–7.72 (m, 2H, Ar).

*4-Methoxyphenyl methyl sulfoxide* (Table 2, entry 2) [122].  $^1\text{H}$  NMR ( $\text{CDCl}_3$ , 300 MHz): 2.70 (s, 3H,  $\text{CH}_3$ ), 3.82 (s, 3H,  $\text{OCH}_3$ ), 7.04–7.10 (m, 2H, Ar), 7.59–7.68 (m, 2H, Ar).

*Methyl 4-nitrophenyl sulfoxide* (Table 2, entry 3) [123].  $^1\text{H}$  NMR ( $\text{CDCl}_3$ , 300 MHz): 2.81 (s, 3H,  $\text{CH}_3$ ), 7.79–7.88 (m, 2H, Ar), 8.37–8.44 (m, 2H, Ar).

*Diphenyl sulfoxide* (Table 2, entry 4) [124].  $^1\text{H}$  NMR ( $\text{CDCl}_3$ , 300 MHz): 7.29–7.43 (m, 6H, Ar), 7.56 (m, 4H, Ar).

*Dibutyl sulfoxide* (Table 2, entry 5) [122]. 0.96 (t,  $J = 7.3$  Hz, 3H,  $\text{CH}_3$ ), 1.36–1.61 (m, 2H,  $\text{CH}_2$ ), 1.65–1.83 (m, 2H,  $\text{CH}_2$ ), 2.60–2.78 (m, 2H,  $\text{CH}_2$ ).

*Thian-4-one S-oxide* (Table 2, entry 6) [125].  $^1\text{H}$  NMR ( $\text{CDCl}_3$ , 300 MHz): 2.43–2.58 (m, 2H,  $\text{CH}_2$ ), 2.78–2.95 (m, 2H,  $\text{CH}_2$ ), 3.19–3.39 (m, 4H,  $2\text{CH}_2$ ).

*(Phenylsulfinyl)acetonitrile* (Table 2, entry 7) [126].  $^1\text{H}$  NMR ( $\text{CDCl}_3$ , 300 MHz): 3.72 (s, 2H,  $\text{CH}_2$ ), 7.49–7.75 (m, 5H, CH).

*(2-Phenylsulfinyl)ethanol* (Table 2, entry 8) [127].  $^1\text{H}$  NMR ( $\text{CDCl}_3$ , 300 MHz): 3.07–3.13 (t, 2H,  $\text{CH}_2\text{S}$ ), 3.72–3.77 (t, 2H,  $\text{CH}_2\text{O}$ ), 7.19–7.28 (m, 3H, *p*-, *m*-CH), 7.35 (d,  $J = 7$  Hz, 2H, *o*-CH).

*Phenyl vinyl sulfide* (Table 2, entry 9) [128].  $^1\text{H}$  NMR ( $\text{CDCl}_3$ , 300 MHz): 5.88 (d,  $J = 9.7$  Hz, 1H,  $\text{CH}_2$ ), 6.18 (d,  $J = 16.4$  Hz, 1H,  $\text{CH}_2$ ), 6.65 (dd,  $J = 16.4, 9.7$  Hz, 1H, CH), 7.44–7.77 (m, 5H, Ar).

*Hot filtration test.* A 15 mL 2-necked flask equipped with a magnetic stir bar was charged with 0.09 mol% of heterogenized  $\text{Mn}(\text{TMPIP})$  (calculations were based on the data of ICP-OES analysis of  $\text{Mn}(\text{TMPIP})/\text{TiO}_2$ ). The reaction vessel was evacuated and purged with oxygen 3 times. Subsequently, 117  $\mu\text{L}$  (1 mmol) of thioanisole, 456  $\mu\text{L}$  (5 mmol) of IBA, and 4 mL of toluene were added by syringe, and the reaction mixture was stirred at room temperature under oxygen (filled balloon) and periodically monitored by GC-MS. When half of the sulfide was consumed, half of the solution (2.2 mL) was withdrawn and filtered using a membrane filter (0.22  $\mu\text{m}$ ). The second 15 mL 2-necked flask equipped with a magnetic stir bar was evacuated and purged by oxygen 3 times. This reaction vessel was charged with the filtered solution obtained as described above and an oxygen-filled balloon. Both reaction mixtures were stirred at room temperature and monitored by GS-MS. The results of GS-MS analyses are shown in Figure S9.

*Catalyst recycling.* A 25 mL 2-necked flask equipped with a magnetic stir bar was charged with 0.09 mol% of heterogenized  $\text{Mn}(\text{TMPIP})$  (calculations were based on the data of ICP-OES analysis of  $\text{Mn}(\text{TMPIP})/\text{TiO}_2$ ). The reaction vessel was evacuated and purged by oxygen 3 times. Subsequently, 293  $\mu\text{L}$  (1 mmol) of thioanisole, 1.139 mL (5 mmol) of IBA, and 10 mL of toluene were added via a syringe, and the reaction mixture was stirred at room temperature under oxygen (filled balloon) and monitored by GC-MS. After complete consumption of thioanisole, the reaction mixture was centrifugated, and the catalyst was washed with toluene ( $3 \times 10$  mL) and dried for 3 h at r.t. The solid thus obtained was used as a catalyst in the next consecutive oxidation cycle. The filtrate was analyzed using GC-MS with naphthalene as an internal standard, evaporated under reduced pressure and analyzed by ICP-OES to determine the content of Mn. The results of these experiments are summarized in Table S3 and shown in Figure 6.

### 3.5. Computational Details

The quantum calculations were carried out with Spartan'10 software (build 1.1.0, Wavefunction Inc., Tokio, Japan) running on a desktop computer with the Windows operating system. The structures were found by convergence to equilibrium geometry at an energy minimum with default values of gradient tolerance ( $4.5 \times 10^{-4}$  Hartree.Bohr<sup>-1</sup>) and distance tolerance ( $1.8 \times 10^{-3}$  Å). The DFT calculations were performed at the B3LYP level of theory with a 6-31G\* basis set. The starting structures for calculation were prepared by minimization with the semi-empirical PM6 method. The vibrational frequencies were calculated to prove the found structures to be minimal and showed no imaginary frequencies.

## 4. Conclusions

*meso*-Tetraarylporphyrins were immobilized on hydrated mesoporous titanium dioxide ( $S_{\text{BET}} = 705 \text{ m}^2 \text{ g}^{-1}$ ) using carboxylate or phosphonate anchoring groups attached to 2-arylimidazole linker fused across one of the pyrrolic rings of the macrocycle. Two types of hybrid materials with different loading of metalloporphyrins were prepared and characterized as both a bulk solid and at the molecular level using different physicochemical methods, including elemental analysis, UV-vis diffusion and infrared spectroscopies, SEM microphotography and nitrogen sorption isotherms. The morphology of these hybrid materials is similar to that of the pristine TiO<sub>2</sub> and is perfectly suited for application of these materials in catalysis. The mesoporous nanospheroids, with a diameter ranging from 5 to 20 nm, are irregularly distributed in space and separated by large holes of hundreds of nanometers, thus providing good accessibility to catalytic sites. The homogeneous distribution of catalytic sites inside mesopores was proven by EDX analysis in STEM mode and studies of N<sub>2</sub> adsorption isotherms. Quantitative immobilization of porphyrin catalysts can be achieved using both carboxylate and phosphonate anchors, but only the latter one gives hybrid materials which are stable in polar and protic solvents commonly used in organic synthesis.

Finally, catalytic properties of the more stable material **Mn(TMPIP)/TiO<sub>2</sub>** with the phosphonate anchor were evaluated in the selective oxidation of sulfides to sulfoxides by the molecular oxygen/IBA system. The heterogenized complex has shown excellent catalytic activity exhibiting a turnover (TON) of ~1100 in a single catalytic run of the sulfoxidation of thioanisole. TON can be increased by recycling the catalysts at least seven times, owing to the exceptional stability of the solid. This catalyst allows for mild reaction conditions, a wide range of substrates, and excellent product yields in the reactions performed in toluene which is tolerated in industry.

Thus, we have developed a novel synthetic approach to the heterogenization of metalloporphyrins. This strategy has many potential benefits for sustainable chemistry technologies. Structural parameters of grafted metalloporphyrins can be fine-tuned by changing the nature of the central metal ion and four aryl substituents attached to the *meso*-positions of the porphyrin core, which is important for the optimization of their catalytic activity. The heterogenized catalysts thus prepared also benefit from the rational design of the spacer, which is a long and rigid residue and provides a perpendicular orientation of the mean porphyrin plane with respect to a solid surface which is highly desirable for the easy accessibility of catalytic sites. The mesoporous titania is a cost-efficient, thermally and chemically stable support that could decrease production costs. Last but not least, the quantity of the catalyst grafted onto the TiO<sub>2</sub> surface can be easily controlled and adapted to the target catalytic reaction allowing for the economic use of expensive porphyrin complexes. We believe that this immobilization strategy will be useful in catalysis because the scope of reactions catalyzed by metalloporphyrins is constantly increased.

**Supplementary Materials:** The following supporting information can be downloaded at: <https://www.mdpi.com/article/10.3390/catal13020402/s1>. Figure S1: UV–vis spectra of **Mn(TMPIC)** (a) and **Mn(TMPIP)** (b) in chloroform solution; Figure S2: HRMS-ESI mass spectrum of **Mn(TMPIC)**; Figure S3: HRMS-ESI mass spectrum of **Mn(TMPIP)**; Figure S4: HRMS-ESI mass spectrum of **Mn(TMPIP-OH)**; Figure S5: EDX spectra in STEM mode of hybrid material **Mn(TMPIP)/TiO<sub>2</sub>**: all studied region (a), the region of 0–0.6 keV (b) the region of 0.6–1.4 keV (c), the results of quantitative analysis (d). Cu is observed because of spurious X-rays coming from the TEM copper grid; Figure S6: FTIR spectra of **Mn(TMPIP)**, **Mn(TMPIP-OH)**, **Mn(TMPIP)/TiO<sub>2</sub>-1** and hydrated TiO<sub>2</sub>; Figure S7: FTIR spectra of **Mn(TMPIC)**, **Mn(TMPIC)/TiO<sub>2</sub>-1**, **Mn(TMPIC)/TiO<sub>2</sub>**, and hydrated TiO<sub>2</sub>; Figure S8: SEM microphotographs of (a) bare hydrated TiO<sub>2</sub>, and (b) **Mn(TMPIP)/TiO<sub>2</sub>**; Figure S9: The hot filtration test for oxidation reaction of thioanisole with molecular oxygen in the presence of **Mn(TMPIP)/TiO<sub>2</sub>** and IBA (Table 2, entry 1); Figure S10: Kubelka-Munk transformed diffuse reflectance spectra of **Mn(TMPIP)/TiO<sub>2</sub>** before and catalytic tests. The solid recovered after the 7th catalytic cycle was analysed. The electronic absorption spectrum of complex **Mn(TMPIP)** in methanol is shown on the inset; Table S1: Chemical composition of solids prepared by grafting **Mn(TMPIP)** and **Mn(TMPIC)**; Table S2: BET surface area, total pore volume and pore diameter for hydrated titania and heterogenized catalysts obtained in this work; Table S3: Recycling of **Mn(TMPIP)/TiO<sub>2</sub>**.

**Author Contributions:** Conceptualization, A.B.-L.; Methodology of porphyrin synthesis and DFT calculations, K.P.B.; Investigation, I.A.A.; TEM and SEM studies, R.C.; Writing, A.B.-L.; Project administration, K.P.B. and A.B.-L.; Funding acquisition, A.B.-L. All authors have read and agreed to the published version of the manuscript.

**Funding:** Financial support from the CNRS, the Conseil Régional de Bourgogne (PARI IME SMT8 and PARI II CDEA programs), and the European Regional Development Fund (FEDER) is acknowledged. This work was carried out in the frame of the International Associated French–Russian Laboratory of Macrocyclic Systems and Related Materials (LIA LAMREM) of CNRS and RAS (2011–2019). I.A. is grateful to the French government and the French embassy in Russia for financial support of a joint Russian–French PhD Thesis (2014–2017).

**Data Availability Statement:** Not applicable.

**Acknowledgments:** The authors are very grateful to Frédéric Herbst for their cooperation in SEM studies and helpful discussions. Stéphane Brandès, Quentin Bonnin, Marie-José Penouilh, Myriam Laly, and Marcel Soustelle are warmly acknowledged for their technical assistance. We also thank A. Cheprakov for fruitful and profitable discussions.

**Conflicts of Interest:** The authors declare no conflict of interest.

## References

1. Lu, W.; Zhou, L. *Oxidation of C–H Bonds*; John Wiley & Sons, Inc.: Hoboken, NJ, USA, 2017; p. 496.
2. Clerici, M.G.; Kholdeeva, O.A. *Liquid Phase Oxidation via Heterogeneous Catalysis: Organic Synthesis and Industrial Applications*; John Wiley & Sons, Inc.: Hoboken, NJ, USA, 2013.
3. Teles, J.H.; Hermans, I.; Franz, G.; Sheldon, R.A. Oxidation. In *Ullmann's Encyclopedia of Industrial Chemistry*; Verlag Chemie: Hoboken, NJ, USA, 2015; pp. 1–103.
4. Mejia, E. (Ed.) *Catalytic Aerobic Oxidations*; The Royal Society of Chemistry: Cambridge, UK, 2020; p. 334.
5. Punniyamurthy, T.; Velusamy, S.; Iqbal, J. Recent advances in transition metal catalyzed oxidation of organic Substrates with molecular oxygen. *Chem. Rev.* **2005**, *105*, 2329–2364. [[CrossRef](#)]
6. Wang, D.; Weinstein, A.B.; White, P.B.; Stahl, S.S. Ligand-promoted palladium-catalyzed aerobic oxidation reactions. *Chem. Rev.* **2018**, *118*, 2636–2679. [[CrossRef](#)] [[PubMed](#)]
7. Mansuy, D. A brief history of the contribution of metalloporphyrin models to cytochrome P450 chemistry and oxidation catalysis. *Comptes Rendus Chim.* **2007**, *10*, 392–413. [[CrossRef](#)]
8. Pereira, M.M.; Dias, L.D.; Calvete, M.J.F. Metalloporphyrins: Bioinspired oxidation catalysts. *ACS Catal.* **2018**, *8*, 10784–10808. [[CrossRef](#)]
9. Groves, J.T.; McClusky, G.A. Aliphatic hydroxylation *via* oxygen rebound. Oxygen transfer catalyzed by iron. *J. Am. Chem. Soc.* **1976**, *98*, 859–861. [[CrossRef](#)]
10. Groves, J.T.; Nemo, T.E.; Myers, R.S. Hydroxylation and epoxidation catalyzed by iron-porphine complexes. Oxygen transfer from iodosylbenzene. *J. Am. Chem. Soc.* **1979**, *101*, 1032–1033. [[CrossRef](#)]
11. Liu, W.; Groves, J.T. Manganese catalyzed C–H Halogenation. *Acc. Chem. Res.* **2015**, *48*, 1727–1735. [[CrossRef](#)]

12. Haber, J.; Młodnicka, T.; Poltowicz, J. Metal-dependent reactivity of some metalloporphyrins in oxidation with dioxygen. *J. Mol. Catal.* **1989**, *54*, 451–461. [[CrossRef](#)]
13. Lu, W.Y.; Bartoli, J.F.; Battioni, P.; Mansuy, D. Selective oxygenation of hydrocarbons and sulfoxidation of thioethers by dioxygen with a Mn-porphyrin-based cytochrome P450 model system using zinc as electron donor. *New J. Chem.* **1992**, *16*, 621–628. [[CrossRef](#)]
14. Guo, C.-C.; Yang, W.-J.; Mao, Y.-L. Selectively aerobic oxidation of CC and allylic CH bonds in  $\alpha$ -pinene over simple metalloporphyrins. *J. Mol. Catal. A Chem.* **2005**, *226*, 279–284. [[CrossRef](#)]
15. Liu, C.; Shen, D.-M.; Chen, Q.-Y. Fluorous biphasic catalytic oxidation of alkenes and aldehydes with air and 2-methylpropanal in the presence of ( $\beta$ -perfluoroalkylated tetraphenylporphyrin)cobalt complexes. *Eur. J. Org. Chem.* **2006**, *2006*, 2703–2706. [[CrossRef](#)]
16. Ji, H.-B.; Yuan, Q.-L.; Zhou, X.-T.; Pei, L.-X.; Wang, L.-F. Highly efficient selective oxidation of alcohols to carbonyl compounds catalyzed by ruthenium (III) meso-tetraphenylporphyrin chloride in the presence of molecular oxygen. *Bioorg. Med. Chem. Lett.* **2007**, *17*, 6364–6368. [[CrossRef](#)] [[PubMed](#)]
17. Meunier, B. Metalloporphyrins as versatile catalysts for oxidation reactions and oxidative DNA cleavage. *Chem. Rev.* **1992**, *92*, 1411–1456. [[CrossRef](#)]
18. Mansuy, D. Activation of alkanes: The biomimetic approach. *Coord. Chem. Rev.* **1993**, *125*, 129–141. [[CrossRef](#)]
19. Dolphin, D.; Traylor, T.G.; Xie, L.Y. Polyhaloporphyrins: Unusual ligands for metals and metal-catalyzed oxidations. *Acc. Chem. Res.* **1997**, *30*, 251–259. [[CrossRef](#)]
20. van der Made, A.W.; Smeets, J.W.H.; Nolte, R.J.M.; Drenth, W. Olefin epoxidation by a mono-oxygenase model. Effect of site isolation. *J. Chem. Soc. Chem. Commun.* **1983**, 1204–1206. [[CrossRef](#)]
21. Nakagaki, S.; Ferreira, G.K.B.; Ucoski, G.M.; Dias de Freitas Castro, K.A. Chemical reactions catalyzed by metalloporphyrin-based metal-organic frameworks. *Molecules* **2013**, *18*, 7279–7308. [[CrossRef](#)]
22. Takagi, S.; Eguchi, M.; Tryk, D.A.; Inoue, H. Porphyrin photochemistry in inorganic/organic hybrid materials: Clays, layered semiconductors, nanotubes, and mesoporous materials. *J. Photochem. Photobiol. C Photochem. Rev.* **2006**, *7*, 104–126. [[CrossRef](#)]
23. Santos, J.S.D.; Faria, A.L.; Amorin, P.M.D.S.; Luna, F.M.L.; Caiado, K.L.; Silva, D.O.C.E.; Sartoratto, P.P.C.; Assis, M.D. Iron(III) porphyrin covalently supported onto magnetic amino-functionalized nanospheres as catalyst for hydrocarbon and herbicide oxidations. *J. Braz. Chem. Soc.* **2012**, *23*, 1411–1420. [[CrossRef](#)]
24. de Lima, O.J.; de Aguirre, D.P.; de Oliveira, D.C.; da Silva, M.A.; Mello, C.; Leite, C.A.P.; Sacco, H.C.; Ciuffi, K.J. Porphyrins entrapped in an alumina matrix. *J. Mater. Chem.* **2001**, *11*, 2476–2481. [[CrossRef](#)]
25. Rayati, S.; Nejabat, F. Catalytic activity of Fe-porphyrins grafted on multiwalled carbon nanotubes in the heterogeneous oxidation of sulfides and degradation of phenols in water. *Comptes Rendus Chim.* **2017**, *20*, 967–974. [[CrossRef](#)]
26. Chino, M.; Leone, L.; Zambrano, G.; Pirro, F.; D’Alonzo, D.; Firpo, V.; Aref, D.; Lista, L.; Maglio, O.; Nastri, F.; et al. Oxidation catalysis by iron and manganese porphyrins within enzyme-like cages. *Biopolymers* **2018**, *109*, e23107. [[CrossRef](#)]
27. Neves, C.M.B.; Rebelo, S.L.H.; Faustino, M.A.F.; Neves, M.G.P.M.S.; Simões, M.M.Q. Second-generation manganese(III) porphyrins bearing 3,5-dichloropyridyl units: Innovative homogeneous and heterogeneous catalysts for the epoxidation of alkenes. *Catalysts* **2019**, *9*, 967. [[CrossRef](#)]
28. Castro, K.A.D.F.; Westrup, K.C.M.; Silva, S.; Pereira, P.M.R.; Simões, M.M.Q.; Neves, M.D.G.P.; Cavaleiro, J.A.S.; Tomé, J.P.C.; Nakagaki, S. Iron(III) Complexation with galactodendritic porphyrin species and hydrocarbons’ oxidative transformations. *Eur. J. Inorg. Chem.* **2021**, *2021*, 2857–2869. [[CrossRef](#)]
29. Qodrati-nasrabadi, F.; Sardivand-chegini, I.; Heydari-turkmani, A.; Zakavi, S. Acid-induced improvement of photosensitizing efficiency of porphyrins under heterogeneous aqueous conditions: High photosensitizing activity, dissociative stability and photooxidative durability. *J. Environ. Chem. Eng.* **2023**, *11*, 109022. [[CrossRef](#)]
30. Bedioui, F. Zeolite-encapsulated and clay-intercalated metal porphyrin, phthalocyanine and Schiff-base complexes as models for biomimetic oxidation catalysts: An overview. *Coord. Chem. Rev.* **1995**, *144*, 39–68. [[CrossRef](#)]
31. Nakagaki, S.; Xavier, C.R.; Wosniak, A.J.; Mangrich, A.S.; Wypych, F.; Cantão, M.P.; Denicoló, I.; Kubota, L.T. Synthesis and characterization of zeolite-encapsulated metalloporphyrins. *Colloids Surf. A* **2000**, *168*, 261–276. [[CrossRef](#)]
32. Nakagaki, S.; Halma, M.; Bail, A.; Arizaga, G.G.; Wypych, F. First insight into catalytic activity of anionic iron porphyrins immobilized on exfoliated layered double hydroxides. *J. Colloid Interface Sci.* **2005**, *281*, 417–423. [[CrossRef](#)]
33. Zhou, X.; Ji, H. Manganese porphyrin immobilized on montmorillonite: A highly efficient and reusable catalyst for the aerobic epoxidation of olefins under ambient conditions. *J. Porphyr. Phthalocyanines* **2012**, *16*, 1032–1039. [[CrossRef](#)]
34. Zhou, X.-T.; Ji, H.-B. Highly efficient selective oxidation of sulfides to sulfoxides by montmorillonite-immobilized metalloporphyrins in the presence of molecular oxygen. *Catal. Commun.* **2014**, *53*, 29–32. [[CrossRef](#)]
35. Nakagaki, S.; Mantovani, K.M.; Sippel Machado, G.; Dias de Freitas Castro, K.A.; Wypych, F. Recent advances in solid catalysts obtained by metalloporphyrins immobilization on layered anionic exchangers: A short review and some new catalytic results. *Molecules* **2016**, *21*, 291. [[CrossRef](#)]
36. Lindsay Smith, J.R.; Yamamoto, Y.; Vinhadó, F.S. Oxidation of alkanes by iodosylbenzene (PhIO) catalysed by supported Mn(III) porphyrins: Activity and mechanism. *J. Mol. Catal. A Chem.* **2006**, *252*, 23–30. [[CrossRef](#)]

37. Vinhado, F.S.; Prado-Manso, C.M.C.; Sacco, H.C.; Yamamoto, Y. Cationic manganese(III) porphyrins bound to a novel bis-functionalised silica as catalysts for hydrocarbons oxygenation by iodosylbenzene and hydrogen peroxide. *J. Mol. Catal. A Chem.* **2001**, *174*, 279–288. [[CrossRef](#)]
38. Aparecida Vidoto, E.; Silvia Monsalves Moreira, M.; da Silva Vinhado, F.; Jorge Ciuffi, K.; Rangel Nascimento, O.; Yamamoto, Y. Immobilization of  $\beta$  halogenated ironporphyrin in the silica matrix by the sol–gel process. *J. Non-Cryst. Solids* **2002**, *304*, 151–159. [[CrossRef](#)]
39. Ucoski, G.M.; Nunes, F.S.; DeFreitas-Silva, G.; Idemori, Y.M.; Nakagaki, S. Metalloporphyrins immobilized on silica-coated Fe<sub>3</sub>O<sub>4</sub> nanoparticles: Magnetically recoverable catalysts for the oxidation of organic substrates. *Appl. Catal. A* **2013**, *459*, 121–130. [[CrossRef](#)]
40. Gao, B.; Chen, Y.; Lei, Q. Hydroxylation of cyclohexane with molecular oxygen catalyzed by highly efficient heterogeneous Mn(III) porphyrin catalysts prepared by special synthesis and immobilization method. *J. Incl. Phenom. Macrocycl. Chem.* **2012**, *74*, 455–465. [[CrossRef](#)]
41. Alkordi, M.H.; Liu, Y.; Larsen, R.W.; Eubank, J.F.; Eddaoudi, M. Zeolite-like metal–organic frameworks as platforms for applications: On metalloporphyrin-based catalysts. *J. Am. Chem. Soc.* **2008**, *130*, 12639–12641. [[CrossRef](#)] [[PubMed](#)]
42. Li, C.; Qiu, W.; Long, W.; Deng, F.; Bai, G.; Zhang, G.; Zi, X.; He, H. Synthesis of porphyrin@MOFs type catalysts through “one-pot” self-assembly. *J. Mol. Catal. A Chem.* **2014**, *393*, 166–170. [[CrossRef](#)]
43. Beyzavi, H.; Vermeulen, N.A.; Howarth, A.J.; Tussupbayev, S.; League, A.B.; Schweitzer, N.M.; Gallagher, J.R.; Platero-Prats, A.E.; Hafezi, N.; Sarjeant, A.A.; et al. A Hafnium-based metal–organic framework as a nature-inspired tandem reaction catalyst. *J. Am. Chem. Soc.* **2015**, *137*, 13624–13631. [[CrossRef](#)]
44. Feng, L.; Wang, Y.; Yuan, S.; Wang, K.-Y.; Li, J.-L.; Day, G.S.; Qiu, D.; Cheng, L.; Chen, W.-M.; Madrahimov, S.T.; et al. Porphyrinic metal–organic frameworks installed with Brønsted acid sites for efficient tandem semisynthesis of artemisinin. *ACS Catal.* **2019**, *9*, 5111–5118. [[CrossRef](#)]
45. Chen, L.; Yang, Y.; Jiang, D. CMPs as scaffolds for constructing porous catalytic frameworks: A built-in heterogeneous catalyst with high activity and selectivity based on nanoporous metalloporphyrin polymers. *J. Am. Chem. Soc.* **2010**, *132*, 9138–9143. [[CrossRef](#)] [[PubMed](#)]
46. Amadelli, R.; Bregola, M.; Polo, E.; Carassiti, V.; Maldotti, A. Photooxidation of hydrocarbons on porphyrin-modified titanium dioxide powders. *J. Chem. Soc. Chem. Commun.* **1992**, 1355–1357. [[CrossRef](#)]
47. Mantovani, K.M.; Stival, J.F.; Wypych, F.; Bach, L.; Peralta Zamora, P.G.; Luiza Rocco, M.; Nakagaki, S. Unusual catalytic activity after simultaneous immobilization of two metalloporphyrins on hydrozincite/nanocrystalline anatase. *J. Catal.* **2017**, *352*, 442–451. [[CrossRef](#)]
48. Machado, G.S.; Ucoski, G.M.; de Lima, O.J.; Ciuffi, K.J.; Wypych, F.; Nakagaki, S. Cationic and anionic metalloporphyrins simultaneously immobilized onto raw halloysite nanoscrolls catalyze oxidation reactions. *Appl. Catal. A* **2013**, *460–461*, 124–131. [[CrossRef](#)]
49. Machado, G.S.; Arizaga, G.G.C.; Wypych, F.; Nakagaki, S. Immobilization of anionic metalloporphyrins on zinc hydroxide nitrate and study of an unusual catalytic activity. *J. Catal.* **2010**, *274*, 130–141. [[CrossRef](#)]
50. Perego, C.; Millini, R. Porous materials in catalysis: Challenges for mesoporous materials. *Chem. Soc. Rev.* **2013**, *42*, 3956–3976. [[CrossRef](#)] [[PubMed](#)]
51. Suib, S.L.; Přeč, J.; Čejka, J.; Kuwahara, Y.; Mori, K.; Yamashita, H. Some novel porous materials for selective catalytic oxidations. *Mater. Today* **2020**, *32*, 244–259. [[CrossRef](#)]
52. El Mourabit, S.; Guillot, M.; Toquer, G.; Cambedouzou, J.; Goettmann, F.; Grandjean, A. Stability of mesoporous silica under acidic conditions. *RSC Adv.* **2012**, *2*, 10916–10924. [[CrossRef](#)]
53. Yang, S.-A.; Choi, S.; Jeon, S.M.; Yu, J. Silica nanoparticle stability in biological media revisited. *Sci. Rep.* **2018**, *8*, 185. [[CrossRef](#)]
54. Pereira, C.F.; Simões, M.M.Q.; Tomé, J.P.C.; Almeida Paz, F.A. Porphyrin-Based metal-organic frameworks as heterogeneous catalysts in oxidation reactions. *Molecules* **2016**, *21*, 1348. [[CrossRef](#)]
55. Yakushev, A.A.; Abel, A.S.; Averin, A.D.; Beletskaya, I.P.; Cheprakov, A.V.; Ziankou, I.S.; Bonneviot, L.; Bessmertnykh-Lemeune, A. Visible light photocatalysis promoted by solid- and liquid-phase immobilized transition metal complexes in organic synthesis. *Coord. Chem. Rev.* **2022**, *458*, 214331. [[CrossRef](#)]
56. Crossley, M.J.; McDonald, J.A. Fused porphyrin-imidazole systems: New building blocks for synthesis of porphyrin arrays. *J. Chem. Soc. Perkin Trans. 1* **1999**, *17*, 2429–2431. [[CrossRef](#)]
57. Abdulaeva, I.A.; Birin, K.P.; Bessmertnykh-Lemeune, A.; Tsvadze, A.Y.; Gorbunova, Y.G. Heterocycle-appended porphyrins: Synthesis and challenges. *Coord. Chem. Rev.* **2020**, *407*, 213108. [[CrossRef](#)]
58. Abdulaeva, I.A.; Birin, K.P.; Michalak, J.; Romieu, A.; Stern, C.; Bessmertnykh-Lemeune, A.; Guillard, R.; Gorbunova, Y.G.; Tsvadze, A.Y. On the synthesis of functionalized porphyrins and porphyrin conjugates via  $\beta$ -aminoporphyrins. *New J. Chem.* **2016**, *40*, 5758–5774. [[CrossRef](#)]
59. Barona-Castaño, J.C.; Carmona-Vargas, C.C.; Brocksom, T.J.; De Oliveira, K.T. Porphyrins as catalysts in scalable organic reactions. *Molecules* **2016**, *21*, 310. [[CrossRef](#)]
60. Adler, A.D.; Longo, F.R.; Kampas, F.; Kim, J. On the preparation of metalloporphyrins. *J. Inorg. Nucl. Chem.* **1970**, *32*, 2443–2445. [[CrossRef](#)]
61. Boucher, L.J. Manganese porphyrin complexes. *Coord. Chem. Rev.* **1972**, *7*, 289–329. [[CrossRef](#)]

62. Fagadar-Cosma, E.; Mirica, M.C.; Balcu, I.; Bucovicean, C.; Cretu, C.; Armeanu, I.; Fagadar-Cosma, G. Syntheses, spectroscopic and AFM characterization of some manganese porphyrins and their hybrid silica nanomaterials. *Molecules* **2009**, *14*, 1370–1388. [[CrossRef](#)]
63. Queffelec, C.; Petit, M.; Janvier, P.; Knight, D.A.; Bujoli, B. Surface modification using phosphonic acids and esters. *Chem. Rev.* **2012**, *112*, 3777–3807. [[CrossRef](#)]
64. Guerrero, G.; Alauzun, J.G.; Granier, M.; Laurencin, D.; Mutin, P.H. Phosphonate coupling molecules for the control of surface/interface properties and the synthesis of nanomaterials. *Dalton Trans.* **2013**, *42*, 12569–12585. [[CrossRef](#)]
65. Zhu, Y.-P.; Ma, T.-Y.; Liu, Y.-L.; Ren, T.-Z.; Yuan, Z.-Y. Metal phosphonate hybrid materials: From densely layered to hierarchically nanoporous structures. *Inorg. Chem. Front.* **2014**, *1*, 360–383. [[CrossRef](#)]
66. Cattani-Scholz, A. Functional organophosphonate interfaces for nanotechnology: A review. *ACS Appl. Mater. Interfaces* **2017**, *9*, 25643–25655. [[CrossRef](#)]
67. Maillot, C.; Janvier, P.; Pipelier, M.; Praveen, T.; Andres, Y.; Bujoli, B. Hybrid materials for catalysis? Design of new phosphonate-based supported catalysts for the hydrogenation of ketones under hydrogen pressure. *Chem. Mater.* **2001**, *13*, 2879–2884. [[CrossRef](#)]
68. Maillot, C.; Janvier, P.; Bertrand, M.-J.; Praveen, T.; Bujoli, B. Phosphonate-based hybrid materials for catalysis? Supported rhodium/2,2'-bipyridine complexes as reduction catalysts under hydrogen pressure. *Eur. J. Org. Chem.* **2002**, *2002*, 1685–1689. [[CrossRef](#)]
69. Schull, T.L.; Henley, L.; Deschamps, J.R.; Butcher, R.J.; Maher, D.P.; Klug, C.A.; Swider-Lyons, K.; Dressick, W.J.; Bujoli, B.; Greenwood, A.E.; et al. Organometallic supramolecular mixed-valence cobalt(I)/cobalt(II) aquo complexes stabilized with the water-soluble phosphine ligand *p*-TPPTP (*p*-triphenylphosphine triphosphonic acid). *Organometallics* **2007**, *26*, 2272–2276. [[CrossRef](#)]
70. Guerrero, G.; Mutin, P.H.; Framery, E.; Vioux, A. Immobilization of platinum(II) and palladium(II) complexes on metal oxides by sol-gel processing and surface modification using bifunctional phosphine-phosphonate esters. *New J. Chem.* **2008**, *32*, 1519–1525. [[CrossRef](#)]
71. Forato, F.; Belhboub, A.; Monot, J.; Petit, M.; Benoit, R.; Sarou-Kanian, V.; Fayon, F.; Jacquemin, D.; Queffelec, C.; Bujoli, B. Phosphonate-mediated immobilization of rhodium/bipyridine hydrogenation catalysts. *Chem.-Eur. J.* **2018**, *24*, 2457–2465. [[CrossRef](#)]
72. Forato, F.; Talebzadeh, S.; Bujoli, B.; Queffelec, C.; Trammell, S.A.; Knight, D.A. Core-Shell Ag@TiO<sub>2</sub> nanocomposites for low-power blue laser enhanced copper(I) catalyzed Ullmann coupling. *ChemistrySelect* **2017**, *2*, 769–773. [[CrossRef](#)]
73. Zhu, Y.-P.; Ren, T.-Z.; Yuan, Z.-Y. Insights into mesoporous metal phosphonate hybrid materials for catalysis. *Catal. Sci. Technol.* **2015**, *5*, 4258–4279. [[CrossRef](#)]
74. Bhanja, P.; Bhaumik, A. Organic-inorganic hybrid metal phosphonates as recyclable heterogeneous catalysts. *ChemCatChem* **2016**, *8*, 1607–1616. [[CrossRef](#)]
75. Zhang, L.; Cole, J.M. Anchoring groups for dye-sensitized solar cells. *ACS Appl. Mater. Interfaces* **2015**, *7*, 3427–3455. [[CrossRef](#)]
76. Mitrofanov, A.; Brandes, S.; Herbst, F.; Rigolet, S.; Bessmertnykh-Lemeune, A.; Beletskaya, I. Immobilization of copper complexes with (1,10-phenanthroline)phosphonates on titania supports for sustainable catalysis. *J. Mater. Chem. A* **2017**, *5*, 12216–12235. [[CrossRef](#)]
77. DiGiacomo, P.M.; Dines, M.B. Nonaqueous Preparation of Layered or Amorphous Organometallic Inorganic Polymers. U.S. Patent 4299943, 10 November 1981.
78. Guerrero, G.; Mutin, P.H.; Vioux, A. Anchoring of phosphonate and phosphinate coupling molecules on titania particles. *Chem. Mater.* **2001**, *13*, 4367–4373. [[CrossRef](#)]
79. Kamm, J.M.; Iverson, C.P.; Lau, W.-Y.; Hopkins, M.D. Axial ligand effects on the structures of self-assembled gallium-porphyrin monolayers on highly oriented pyrolytic graphite. *Langmuir* **2016**, *32*, 487–495. [[CrossRef](#)]
80. Yamada, T.; Takai, T.; Rhode, O.; Mukaiyama, T. Highly efficient method for epoxidation of olefins with molecular oxygen and aldehydes catalyzed by nickel(II) complexes. *Chem. Lett.* **1991**, *20*, 1–4. [[CrossRef](#)]
81. Murahashi, S.-I.; Naota, T.; Komiyama, N. Metalloporphyrin-catalyzed oxidation of alkanes with molecular oxygen in the presence of acetaldehyde. *Tetrahedron Lett.* **1995**, *36*, 8059–8062. [[CrossRef](#)]
82. Mastrorilli, P.; Nobile, C.F. Catalytic activity of a polymerizable tris( $\beta$ -ketoesterate)iron(III) complex towards the oxidation of organic substrates. *Tetrahedron Lett.* **1994**, *35*, 4193–4196. [[CrossRef](#)]
83. Brown, J.W.; Nguyen, Q.T.; Otto, T.; Jarenwattananon, N.N.; Glöggler, S.; Bouchard, L.-S. Epoxidation of alkenes with molecular oxygen catalyzed by a manganese porphyrin-based metal-organic framework. *Catal. Commun.* **2015**, *59*, 50–54. [[CrossRef](#)]
84. Malko, D.; Guo, Y.; Jones, P.; Britovsek, G.; Kucernak, A. Heterogeneous iron containing carbon catalyst (Fe-N/C) for epoxidation with molecular oxygen. *J. Catal.* **2019**, *370*, 357–363. [[CrossRef](#)]
85. Gong, M.; Guo, Y.; Malko, D.; Rubio-Garcia, J.; Dawson, J.M.S.; Britovsek, G.J.P.; Kucernak, A. Using molecular oxygen and Fe-N/C heterogeneous catalysts to achieve Mukaiyama epoxidations via in situ produced organic peroxy acids and acylperoxy radicals. *Catal. Sci. Technol.* **2022**, *12*, 2978–2989. [[CrossRef](#)]
86. Rahimi, R.; Gholamrezapor, E.; Naimi-jamal, M.R. Oxidation of benzyl alcohols to the corresponding carbonyl compounds catalyzed by copper (II) meso-tetraphenylporphyrin as cytochrome P-450 model reaction. *Inorg. Chem. Commun.* **2011**, *14*, 1561–1568. [[CrossRef](#)]

87. Chen, L.; Yang, Y.; Guo, Z.; Jiang, D. Highly efficient activation of molecular oxygen with nanoporous metalloporphyrin frameworks in heterogeneous systems. *Adv. Mater.* **2011**, *23*, 3149–3154. [[CrossRef](#)]
88. Miller, S. ES&T Views: In a faraway state. *Environ. Sci. Technol.* **1990**, *24*, 1286–1289.
89. Stingl, K.A.; Tsogoeva, S.B. Recent advances in sulfoxidation reactions: A metal-free approach. *Tetrahedron Asymmetry* **2010**, *21*, 1055–1074. [[CrossRef](#)]
90. Liu, Y.; Howarth, A.J.; Hupp, J.T.; Farha, O.K. Selective photooxidation of a mustard-gas simulant catalyzed by a porphyrinic metal–organic framework. *Angew. Chem. Int. Ed.* **2015**, *54*, 9001–9005. [[CrossRef](#)] [[PubMed](#)]
91. Lang, X.; Hao, W.; Leow, W.R.; Li, S.; Zhao, J.; Chen, X. Tertiary amine mediated aerobic oxidation of sulfides into sulfoxides by visible-light photoredox catalysis on TiO<sub>2</sub>. *Chem. Sci.* **2015**, *6*, 5000–5005. [[CrossRef](#)]
92. Sipos, G.; Drinkel, E.E.; Dorta, R. The emergence of sulfoxides as efficient ligands in transition metal catalysis. *Chem. Soc. Rev.* **2015**, *44*, 3834–3860. [[CrossRef](#)]
93. Laudadio, G.; Straathof, N.J.W.; Lanting, M.D.; Knoops, B.; Hessel, V.; Noël, T. An environmentally benign and selective electrochemical oxidation of sulfides and thiols in a continuous-flow microreactor. *Green Chem.* **2017**, *19*, 4061–4066. [[CrossRef](#)]
94. Jiang, X. (Ed.) *Sulfur Chemistry*; Springer: Berlin, Germany, 2019.
95. Matavos-Aramyan, S.; Soukhakian, S.; Jazebizadeh, M.H. Selected methods for the synthesis of sulfoxides and sulfones with emphasis on oxidative protocols. *Phosphorus Sulfur Silicon Relat. Elem.* **2020**, *195*, 181–193. [[CrossRef](#)]
96. Baciocchi, E.; Rol, C.; Scamosci, E.; Sebastiani, G.V. Medium and structure effects on the anodic oxidation of aryl arylmethyl sulfides. *J. Org. Chem.* **1991**, *56*, 5498–5502. [[CrossRef](#)]
97. Baciocchi, E.; Crescenzi, C.; Lanzalunga, O. Photoinduced electron transfer reactions of benzyl phenyl sulfides promoted by 9,10-dicyanoanthracene. *Tetrahedron* **1997**, *53*, 4469–4478. [[CrossRef](#)]
98. Baciocchi, E.; Del Giacco, T.; Gerini, M.F.; Lanzalunga, O. Rates of C–S bond cleavage in *tert*-alkyl phenyl sulfide radical cations. *Org. Lett.* **2006**, *8*, 641–644. [[CrossRef](#)]
99. Mata, E.G. Recent advances in the synthesis of sulfoxides from sulfides. *Phosphorus Sulfur Silicon Relat. Elem.* **1996**, *117*, 231–286. [[CrossRef](#)]
100. Legros, J.; Dehli, J.R.; Bolm, C. Applications of catalytic asymmetric sulfide oxidations to the syntheses of biologically active sulfoxides. *Adv. Synth. Catal.* **2005**, *347*, 19–31. [[CrossRef](#)]
101. Srouf, H.; Le Maux, P.; Chevance, S.; Simonneaux, G. Metal-catalyzed asymmetric sulfoxidation, epoxidation and hydroxylation by hydrogen peroxide. *Coord. Chem. Rev.* **2013**, *257*, 3030–3050. [[CrossRef](#)]
102. Khanna, V.; Maikap, G.C.; Iqbal, J. An efficient oxidation of sulfides to sulfones using 2-methylpropanal and dioxygen. *Tetrahedron Lett.* **1996**, *37*, 3367–3370. [[CrossRef](#)]
103. Tumula, V.R.; Bondwal, S.; Bisht, P.; Pendem, C.; Kumar, J. Oxidation of sulfides to sulfones with hydrogen peroxide in the presence of acetic acid and Amberlyst 15. *React. Kinet. Mech. Catal.* **2012**, *107*, 449–466. [[CrossRef](#)]
104. Morozkov, G.V.; Abel, A.S.; Filatov, M.A.; Nefedov, S.E.; Roznyatovsky, V.A.; Cheprakov, A.V.; Mitrofanov, A.Y.; Ziankou, I.S.; Averin, A.D.; Beletskaya, I.P.; et al. Ruthenium(II) complexes with phosphonate-substituted phenanthroline ligands: Synthesis, characterization and use in organic photocatalysis. *Dalton Trans.* **2022**, *51*, 13612–13630. [[CrossRef](#)] [[PubMed](#)]
105. Tabushi, I. Reductive dioxygen activation by use of artificial P-450 systems. *Coord. Chem. Rev.* **1988**, *86*, 1–42. [[CrossRef](#)]
106. Laszlo, P.; Levart, M. “Clayniac”-catalyzed epoxidation: The role of the aldehyde as co-reducer of molecular oxygen. *Tetrahedron Lett.* **1993**, *34*, 1127–1130. [[CrossRef](#)]
107. Wentzel, B.B.; Gosling, P.A.; Feiters, M.C.; Nolte, R.J.M. Mechanistic studies on the epoxidation of alkenes with molecular oxygen and aldehydes catalysed by transition metal– $\beta$ -diketonate complexes. *J. Chem. Soc. Dalton Trans.* **1998**, *13*, 2241–2246. [[CrossRef](#)]
108. Boring, E.; Geletii, Y.V.; Hill, C.L. Catalysts for selective aerobic oxidation under ambient conditions. In *Advances in Catalytic Activation of Dioxygen by Metal Complexes*; Simándi, L.I., Ed.; Springer: Boston, MA, USA, 2002; pp. 227–264.
109. Livingston, S.R.; Landry, C.C. Oxidation of a mustard gas analogue using an aldehyde/O<sub>2</sub> system catalyzed by V-doped mesoporous silica. *J. Am. Chem. Soc.* **2008**, *130*, 13214–13215. [[CrossRef](#)] [[PubMed](#)]
110. Zhou, X.; Ji, H. Biomimetic kinetics and mechanism of cyclohexene epoxidation catalyzed by metalloporphyrins. *Chem. Eng. J.* **2010**, *156*, 411–417. [[CrossRef](#)]
111. Lanucara, F.; Crestoni, M.E. Biomimetic oxidation reactions of a naked manganese(V)-oxo porphyrin complex. *Chem.-Eur. J.* **2011**, *17*, 12092–12100. [[CrossRef](#)] [[PubMed](#)]
112. Klaine, S.; Bratcher, F.; Winchester, C.M.; Zhang, R. Formation and kinetic studies of manganese(IV)-oxo porphyrins: Oxygen atom transfer mechanism of sulfide oxidations. *J. Inorg. Biochem.* **2020**, *204*, 110986. [[CrossRef](#)]
113. Xiang, G.; Wu, D.; He, J.; Wang, X. Acquired pH-responsive and reversible enrichment of organic dyes by peroxide modified ultrathin TiO<sub>2</sub> nanosheets. *Chem. Commun.* **2011**, *47*, 11456–11458. [[CrossRef](#)]
114. Moghadam, M.; Tangestaninejad, S.; Mirkhani, V.; Mohammadpoor-Baltork, I.; Abbasi-Larki, A.A. Biomimetic oxidation of sulfides with sodium periodate catalyzed by polystyrene-bound manganese(III) tetrapyridylporphyrin. *Appl. Catal. A* **2008**, *349*, 177–181. [[CrossRef](#)]
115. Mirkhani, V.; Moghadam, M.; Tangestaninejad, S.; Mohammadpoor-Baltork, I.; Kargar, H.; Araghi, M. Highly efficient oxidation of sulfides with sodium periodate catalyzed by reusable silica supported Mn(Br<sub>8</sub>TPP)Cl and Mn(TPP)Cl catalysts under various reaction conditions. *Appl. Catal. A* **2009**, *353*, 61–67. [[CrossRef](#)]



116. Rayati, S.; Rezaie, S.; Nejabat, F. Catalytic activity of Mn(III) porphyrins supported onto graphene oxide nano-sheets for green oxidation of sulfides. *J. Coord. Chem.* **2019**, *72*, 1466–1479. [[CrossRef](#)]
117. Rezaeifard, A.; Jafarpour, M. The catalytic efficiency of Fe-porphyrins supported on multi-walled carbon nanotubes in the heterogeneous oxidation of hydrocarbons and sulfides in water. *Catal. Sci. Technol.* **2014**, *4*, 1960–1969. [[CrossRef](#)]
118. Deniaud, D.; Spyroulias, G.A.; Bartoli, J.-F.; Battioni, P.; Mansuy, D.; Pinel, C.; Odobel, F.; Bujoli, B. Shape selectivity for alkane hydroxylation with a new class of phosphonate-based heterogenised manganese porphyrins. *New J. Chem.* **1998**, *22*, 901–905. [[CrossRef](#)]
119. Benítez, I.O.; Bujoli, B.; Camus, L.J.; Lee, C.M.; Odobel, F.; Talham, D.R. Monolayers as models for supported catalysts: Zirconium phosphonate films containing manganese(III) porphyrins. *J. Am. Chem. Soc.* **2002**, *124*, 4363–4370. [[CrossRef](#)] [[PubMed](#)]
120. Eu, S.; Hayashi, S.; Umeyama, T.; Matano, Y.; Araki, Y.; Imahori, H. Quinoxaline-fused porphyrins for dye-sensitized solar cells. *J. Phys. Chem. C* **2008**, *112*, 4396–4405. [[CrossRef](#)]
121. Kálmán, F.K.; Woods, M.; Caravan, P.; Jurek, P.; Spiller, M.; Tircsó, G.; Király, R.; Brücher, E.; Sherry, A.D. Potentiometric and relaxometric properties of a gadolinium-based MRI contrast agent for sensing tissue pH. *Inorg. Chem.* **2007**, *46*, 5260–5270. [[CrossRef](#)] [[PubMed](#)]
122. Neveselý, T.; Svobodová, E.; Chudoba, J.; Sikorski, M.; Cibulka, R. Efficient Metal-free aerobic photooxidation of sulfides to sulfoxides mediated by a vitamin B<sub>2</sub> derivative and visible light. *Adv. Synth. Catal.* **2016**, *358*, 1654–1663. [[CrossRef](#)]
123. Kamata, K.; Hirano, T.; Mizuno, N. Highly efficient oxidation of sulfides with hydrogen peroxide catalyzed by [SeO<sub>4</sub>{WO(O<sub>2</sub>)<sub>2</sub>}<sub>2</sub>]<sup>2-</sup>. *Chem. Commun.* **2009**, 3958–3960. [[CrossRef](#)]
124. Hosseini-Eshbala, F.; Sedrpoushan, A.; Dehdashti, M.N.; Breit, B.; Mohanazadeh, F.; Veisi, H. Needle ball-like nanostructured mixed Cu-Ni-Co oxides: Synthesis, characterization and application to the selective oxidation of sulfides to sulfoxides. *Mater. Sci. Eng. C* **2019**, *103*, 109814. [[CrossRef](#)]
125. Gao, Y.; Lam, Y. Polymer-supported *N*-phenylsulfonyloxaziridine (Davis reagent): A versatile oxidant. *Adv. Synth. Catal.* **2008**, *350*, 2937–2946. [[CrossRef](#)]
126. Numata, T.; Itoh, O.; Yoshimura, T.; Oae, S. Intramolecular stereospecific Pummerer reactions of aryl (substitutedmethyl) sulfoxides bearing electron-withdrawing groups with acetic anhydride. *Bull. Chem. Soc. Jpn.* **1983**, *56*, 257–265. [[CrossRef](#)]
127. Rostami, A.; Moradi, S.; Shokri, Z. Fe<sub>3</sub>O<sub>4</sub> as a magnetically reusable Fenton nanocatalyst for the oxidation of thiols to sulfonic acid and sulfides to sulfoxides and sulfones. *Comptes Rendus Chim.* **2018**, *21*, 80–87. [[CrossRef](#)]
128. Lindén, A.A.; Krüger, L.; Bäckvall, J.-E. Highly selective sulfoxidation of allylic and vinylic sulfides by hydrogen peroxide using a flavin as catalyst. *J. Org. Chem.* **2003**, *68*, 5890–5896. [[CrossRef](#)] [[PubMed](#)]

**Disclaimer/Publisher's Note:** The statements, opinions and data contained in all publications are solely those of the individual author(s) and contributor(s) and not of MDPI and/or the editor(s). MDPI and/or the editor(s) disclaim responsibility for any injury to people or property resulting from any ideas, methods, instructions or products referred to in the content.